THE LINEARIZED WING THEORY OF THE SUPERSONIC FLOW WITH THE KARMAN'S FOURIER INTEGRAL METHOD

Thesis by

Chieh-Chien Chang

In Partial Fulfillment of the Requirements

for the Degree of

Doctor of Philosophy

California Institute of Technology

Pasadena, California

1950

ACKNOWLEDGEMENT

The writer wishes to express deep appreciation to Professor Theodore von Kármán for his suggestion of this problem, and for his constant guidance and inspiration throughout the work. He wishes also to express his gratitude to Professor H. S. Tsien for his advice and encouragement, particularly in the early part of the development.

The calculations and the drawings have been done by Miss V. O'Brien and Miss P. Clarken, and this aid is gratefully acknowledged.

SUMMARY

Part I gives a short introduction and some physical interpretation of von Kármán's Fourier integral method applied to the supersonic wing theory. A short review of other current contributions to the linearized supersonic wing theory is also given.

Part II presents the general formulation of the von Kármán method from the view-point of the elementary harmonic sources and doublets. First, the disturbance potential and the velocity components of a general flat body with symmetrical airfoil are derived. Next, the disturbance potential of the lifting surface is presented. In contrast to the well-known conical flow method, the von Kármán's Fourier integral method can treat a complicated plan-form as a whole, without considering the detailed geometry, as long as the airfoil sections are similar.

Part III applies the method to the investigation of the wave drag of the non-lifting wing in supersonic flight. A general solution of the wave drag is obtained for the wing with a diamond-shaped airfoil. This solution allows a free choice of a number of the important geometrical parameters. For instance, the wing may be swept forward or backward, tapered or reversed tapered to any ratio. A number of the limiting cases are also investigated. For the practical aerodynamic problems, two useful families of wing plan-form with the fixed taper ratios 0.2 and 0.5, any swept angle, aspect ratio and Mach number are shown in the graphs. A particular application is demonstrated.

The reversed flow theorem on wave drag as shown by von Kármán and Hayes checks well with the consequence of the general solution. This method shows a certain elegance as no conical flow assumption is needed, and the mathematics is powerful enough to obtain a general solution covering all possible geometrical arrangements without detailed considerations.

While in recent years, the direct problem of finding the lift distribution with given angle of attack on the wing has been well solved by the method of conical flow and others, the present treatment in Part IV, on the other hand, investigates the inverse problem, i.e., to find the downwash distribution in the plane of the wing with a pre-assigned lift distribution. This is particularly favorable with the present method. The general solution of the downwash of the tapered swept wings is derived for the case that a constant lift distribution on the wing is pre-assigned. Of course, the method may be applied to any lift or pressure distribution along the wing chord and span. The corresponding angle of attack on the wing and the downwash can be determined everywhere in the plane of the wing. To demonstrate the downwash distribution as given by the general solution, graphs are given to show the downwash of a number of wings including a swept-back tapered wing with supersonic trailing edge and a delta wing.

TABLE OF CONTENTS

I. Introduction

In 1935 von Kármán first showed that the concept of Fourier integral can be adopted to explain the similarity of Prandtl-wing theory and the theory of planning surfaces (Ref. 1). In 1946, von Kármán introduced the Fourier integral method to the supersonic wing theory*. The present author under his guidance investigated this problem to a certain extent and some of the results have been published (Ref. 2, 20). This report may be considered as an extension of the earlier work. As no published literature is available at this moment, some of Prof. von Kármán's work is repeated.

As far as the linearized theory on supersonic wings is concerned, the conical flow method was originated by A. Buseman (Ref. 3) and later reproduced and extended by Lagerstrom (Ref. 4), Hayes (Ref. 5) and Stewart (Ref. 6), Laporte and Bartel (Ref. 7) and Snow (Ref. 8). Each of the later investigators approached the same method with slightly different techniques but confirmed the essential results of Busemann. Before the conical flow method was known in this country, Jones visualized the advantages of the conical flow and showed some of the basic physical concepts (Ref. 9) in 1945. Later in 1946, with the concept of conical flow, Jones also showed the invariance of the Lorentz transformation and introduced the oblique coordinate in the swept wing problem (Ref. 10).

---

*An unpublished report of Northrop Aircraft Company. There is another unpublished report by H. R. Lawrence of the same company on the same subject, which is not available to the author owing to restriction.

The challenge of supersonic flight has aroused the interest of many other investigators. Puckett showed that the source integration method could be applied to study the wave drag problem (Ref. 11). Later Evaard extended this method to solve the lift problem of a finite wing of any planform (Refs. 12 and 13). Heaslet, Lomax and Jones extended Volterra's and Hadamard's method to the supersonic wing problem (Refs. 14 and 15). Gunn in England applied the operational calculus to the same problem (Ref. 17). There are many other works, all of which cannot be mentioned in this paper.

On the other hand, the basic concept of the Fourier integral method is quite different from the above methods. Instead of the concept of conical flow or simple sources and doublets, the present method considers along the direction of flight infinitely long harmonic source (or doublet) lines, the behaviour of which is quite equivalent to the harmonic acoustic source (or doublet) in the sequence of time. Each of such source lines will send out a divergent cylindrical wave in the radial direction. The potential of such a wave can be expressed by the product of the source-strength function and the Hankel function of the second kind. For each Eigen value or frequency of the source oscillation, there is a corresponding Eigen value in the argument of the Hankel function. By means of the principle of superposition, an arbitrary distribution can be synthesized with such simple harmonic sources of different frequencies, if the frequency spectrum is a continuous one. The most powerful technique to serve such a purpose is the Fourier integral method.

Now in the finite wing problem, the boundary is considered as a source sheet rather than as source lines. Such a sheet can be built up by integrating elements of a source strip which is equivalent to a source line in behaviour.

The above simple physical interpretation may help to give some insight into the mathematical theory to be discussed later.

The present paper first tries to give an introduction to von Kármán's method in terms of the physical rather than mathematical approach. Then, the wave drag of a tapered swept-back wing is treated. This work is not a duplication of some other concurrent investigators (Refs. 18, 19, and 21), but rather a supplementary contribution.

The next step is the lift problem. For a given angle of attack, on an arbitrary wing planform it is rather difficult to solve the integral equation analytically. But for a given lift distribution the downwash angle can be evaluated anywhere in the plane of the wing.

The method has a certain elegance. The complete physical effect of the arbitrary wing can be expressed in terms of one integral. The finite number of discontinuous points of the Fourier-Bessel integral gives exactly the right picture. This method is being applied at present, and there are a number of aspects to be extended later.

II. General Theory of the Fourier Integral Method

2.1 The Elementary Solutions.

In the three-dimensional, steady supersonic flow of a compressible non-viscous fluid, the differential equation of motion in the linearized sense is

$$\phi_{yy} + \phi_{zz} = (M^2-1)\,\phi_{xx} \tag{2.1}$$

where the velocity potential ϕ is defined by grad. $\phi = \bar{q} - U\bar{i}$ $= u\bar{i} + v\bar{j} + w\bar{k}$, the disturbance velocity vector. It may be considered as a two-dimensional wave equation if x is conceived as time in the sequence of which the future can contribute nothing to the present. This can be shown clearly by introducing $t \equiv \frac{x}{(M^2-1)^{\frac{1}{2}}}$ i.e.

$$\phi_{yy} + \phi_{zz} = \phi_{tt} \tag{2.2}$$

with the dimension in the flow direction being equivalent to time t. After this transformation, the velocity of propagation in (2.2) is unity. In this sense, Eq. (2.2) becomes the potential problem of the acoustic source and doublet in the (y, z) plane in the sequence of time as pointed out by von Kármán (Ref. 2). After this transformation, the wing planform has to be readjusted so that the Mach waves are inclined backward at 45° from the flow direction. As an example of transformation, Fig. 1 gives a swept-back wing in the physical and transformed planes.

For a simple time-dependent harmonic source with strength $\cos \lambda t$ (where $\frac{\lambda}{2\pi}$ is the frequency of oscillation) located at $(\eta, 0)$ in the (y, z) plane, the elementary solution of Eq. (2.1) as given by Lamb p. 297, (Ref. 17) is

$$\phi_o(t, y, z; \eta, 0) = Re\left[-\frac{i}{4} e^{i\lambda t} H_o^{(2)}(\lambda r)\right] \tag{2.3}$$

where $r = \sqrt{(y-\eta)^2 + z^2}$ and $H_o^{(2)}(\lambda r)$ is the Hankel function of the second kind of zero order. It is easy to show that the solution satisfies both the differential equation (2.2) and the given boundary condition $\cos \lambda t$ = Re. $e^{i\lambda t}$. At very large λr equation (2.3) becomes

$$\phi_o(t, r) \cong \frac{1}{\sqrt{8\pi \lambda r}} \cos\left[\lambda(t-r) - \frac{\pi}{4}\right]$$

the amplitude of which is inversely proportional to the square root of r.

Physically, this represents the potential at the point (y, z) at time t due to a harmonic source of strength $\cos(\lambda t)$ at distance r from it. Such disturbance potential is called a divergent wave. This disturbance propagates from the point $(\eta, 0)$ with a circular or cylindrical symmetry.

Now if the strength of the source is the real part of $F(\lambda)e^{i\lambda t}$ instead of just $e^{i\lambda t}$, the potential must be also written as

$$\phi_o(t,y,z;\eta,0) = Re\left\{-\frac{i}{4}F(\lambda)\,e^{i\lambda t}H_o^{(2)}(\lambda r)\right\}$$

(2.4)

where

$$F(\lambda) = F_o(\lambda) + i\,F_1(\lambda)$$

(2.5)

with $F_o(-\lambda) = F_o(\lambda)$ being even and $F_1(-\lambda) = -F_1(\lambda)$ being odd. It is understood that $F(\lambda)$ is a function representing the strength, amplitude and location of the source line.

If two such harmonic lines source of equal but opposite strength - the negative one located at $(\eta, \frac{-\xi}{2})$ and the positive one at $(\eta, \frac{\xi}{2})$ respectively - approach each other, a harmonic doublet line can be obtained if $\lim_{\xi\to 0} F(\lambda)\cdot\xi = G(\lambda)$ is considered as a finite quantity.

$$\phi_1(t,y,z;\eta,0) = \lim_{\xi\to 0}\left\{\phi_o(t,y,z;\eta,\frac{\xi}{2}) - \phi_o(t,y,z;\eta,\frac{-\xi}{2})\right\}$$

$$= \lim_{\xi\to 0}\frac{\partial\phi_o}{\partial\xi}\cdot\xi = Re\left\{-\frac{i\lambda}{4}G(\lambda)e^{i\lambda t}H_1^{(2)}(\lambda r)\cdot\frac{z}{r}\right\}$$

(2.6)

where the doublet is defined as positive, and

$$G(\lambda) = G_o(\lambda) + i\,G_1(\lambda)$$

(2.7)

with $G_o(-\lambda) = G_o(\lambda)$ being even and $G_1(-\lambda) = -G_1(\lambda)$ being odd.

It is very interesting to see that this potential of the doublet no longer has cylindrical symmetry, but is anti-symmetrical with respect to the (t, y) plane. The harmonic doublet line will be used for the wing lift problem.

2.2. The Boundary Conditions in the Supersonic Wing Problem.

Let a flat body or wing occupy a region in the (x, y) plane and α_+ and α_- are the slopes of the upper and lower wing surfaces at (x, y) respectively. Both are small in comparison to unity and are zero outside the finite region occupied by the wing. Within the approximation of the linearized theory, the wing may be considered equivalent to the superposition of a symmetrical body and a mean-cambered surface. The slope of the symmetrical body is

$$\alpha_o = \frac{1}{2}(\alpha_+ - \alpha_-) \tag{2.8}$$

and the slope of the cambered surface is

$$\alpha_1 = \frac{1}{2}(\alpha_+ + \alpha_-) \tag{2.9}$$

where α_o and α_1 are considered at the (x, y) plane. In other words, the effect of exact location of α_o and α_1 in the z direction is entirely neglected in the future treatment which has been shown by von Kármán to be consistent with the linearized theory for the flat body. From the above, the required boundary condition of the potential is the normal velocity to the wing surface which is zero, i.e.

$$\bar{q} \cdot \bar{n} = 0 \tag{2.10}$$

In this case of a flat body, where the vertical velocity component predominates, equation (2.10) can be approximately expressed by

$$w_+ = \left(\frac{\partial \phi}{\partial z}\right)_{z=+0} = U \cdot \alpha_+ \tag{2.11}$$

$$w_- = \left(\frac{\partial \phi}{\partial z}\right)_{z=-0} = U \cdot \alpha_- \tag{2.12}$$

where w_+ and w_- represent vertical velocity components on the top and bottom of wing surfaces respectively.

Besides, at a distance far away from the wing in the upper stream, $u = v = w = 0$ if there is no other disturbance generated in the upper stream.

2.3. Supersonic Flow about a Flat Symmetrical Body.

If a source line at $(\eta, 0)$ is of any arbitrary strength with finite time t the potential can be built up with Eq. (2.4) by means of a Fourier integral as

$$\phi_o'(t,y,z) = Re \int_{\to 0}^{\infty} d\lambda \left\{ -\frac{Ui}{4} F(\lambda,\eta)\, e^{i\lambda t} H_o^{(2)}(\lambda r) \right\} \tag{2.13}$$

where U is the free stream velocity. The insertion of U in the source strength function is purely for future convenience.

The above integral and its first derivatives exist if the Lebesgue integral

$$\int_0^\infty \lambda \left| F(\lambda,\eta)\, H_0^{(2)}(\lambda r) \right| d\lambda \quad < \infty$$

The above condition is automatically satisfied, if the source with finite strength is in action for a finite time interval. Actually, the equation (2.13) can be considered as the potential of a body of revolution. Sometimes, in conforming with the convention of the complex Fourier integral the above equation may be conveniently written as

$$\phi_0'(t,y,z) = -\frac{Ui}{8} \int_{-\infty}^{\infty} d\lambda\, F(\lambda,\eta)\, e^{i\lambda t} H_0^{(2)}(\lambda r) \tag{2.14}$$

with the understanding that the path of integration of λ is slightly above or below the origin in the complex λ plane so that the singularity at $\lambda = 0$ can be detoured. It can be verified easily because

$$F(-\lambda,\eta) = F_0(\lambda,\eta) - i F_1(\lambda,\eta) = \overline{F(\lambda,\eta)}$$

$$H_0^{(2)}(-\lambda r) = H_0^{(2)}\left\{\lambda r e^{i\pi}\right\} = H_0^{(2)}\left\{\lambda r e^{-i\pi}\right\} = \overline{H_0^{(2)}(\lambda r)}$$

where the 'bar' represents the complex congugate of the original function.

Now, the above source line may be considered as an elementary strip of a source sheet in the (t, y) plane of width $d\eta$ with the above strength as the strength density per unit area. It is clear then that the potential due to a source sheet built up by such strips is

$$\phi_o(t,y,z) = \int_{-\infty}^{\infty} \phi_o' \, d\eta$$

$$= \frac{-Ui}{8} \int_{-\infty}^{\infty} d\eta \int_{-\infty}^{\infty} d\lambda \, F(\lambda,\eta) \, e^{i\lambda t} H_o^{(2)}(\lambda r) \tag{2.15a}$$

For the convenience of the later development, we introduce $f(\lambda,\eta) = -\frac{1}{4} F(\lambda,\eta)$ into equation (2.15a), and then

$$\phi_o(t,y,z) = \frac{Ui}{2} \int_{-\infty}^{\infty} d\eta \int_{-\infty}^{\infty} d\lambda \, f(\lambda,\eta) \, e^{i\lambda t} H_o^{(2)}(\lambda r) \tag{2.15b}$$

One thing should be pointed out. Owing to the structure of the integral, the source sheet may be composed of a number of discontinuous portions in the y direction, and the source strength function f (λ, η) may be different in different discontinuous portions, but it must be the same within one continuous portion of the source sheet. Of course, in that case, the integration with respect to η has to be broken up accordingly. Physically, this integral can give the potential not only due to one wing but a number of wings or flat bodies in (t, y) plane. Therefore, it can be used to study the interaction between wings.

The above equation will be the disturbance potential of the wing, if we can identify the relation of the source strength function $Re\, f(\lambda,\eta)\, e^{i\lambda t}$ with α_0 or the thickness distribution of the symmetrical flat body. This can be obtained from the boundary condition. Differentiating Eq. (2.15) with respect to z we have

$$\frac{\partial \phi_o}{\partial z} = -\frac{Ui}{2}\int_{-\infty}^{\infty} d\eta \int_{-\infty}^{\infty} \lambda\, d\lambda\, f(\lambda,\eta)\, e^{i\lambda t} H_1^{(2)}(\lambda r)\cdot\frac{z}{r} \tag{2.16}$$

Now as $z \to 0$ the integrand goes to zero except in the neighborhood of $\eta = y$. Let $\eta = y + z\tan\theta$; $d\eta = z\sec^2\theta\, d\theta$ where $\theta = \tan^{-1}\frac{\eta - y}{z}$
Besides $H_1^{(2)}(\lambda r) \cong \frac{2i}{\pi\lambda r}$ when λr or $r \to 0$.

Thus Eq. (2.16) becomes

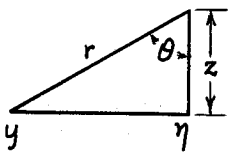

$$(w)_{z=+o} = \left(\frac{\partial \phi_o}{\partial z}\right)_{z=+o}$$

$$= \lim_{z\to+o} \frac{-Ui}{2}\int_{-\infty}^{\infty} d\lambda\, e^{i\lambda t}\int_{-\frac{\pi}{2}}^{\frac{\pi}{2}} \lambda\, f(\lambda, y+z\tan\theta)\frac{2i}{\pi\lambda}\frac{z^2}{r^2}\sec^2\theta\, d\theta$$

$$= \lim_{z\to+o} \frac{U}{\pi}\int_{-\infty}^{\infty} d\lambda\, e^{i\lambda t}\,\lambda\int_{-\frac{\pi}{2}}^{\frac{\pi}{2}} f(\lambda, y+z\tan\theta)\, d\theta$$

$$= \frac{U}{\pi}\int_{-\infty}^{\infty} d\lambda\, e^{i\lambda t} f(\lambda,y)\int_{-\frac{\pi}{2}}^{\frac{\pi}{2}} d\theta = U\int_{-\infty}^{\infty} d\lambda\, f(\lambda,y)\, e^{i\lambda t} \tag{2.17}$$

From Eq. (2.10)

$$(w)_{z=+0} = U\cdot(\alpha_0)_{z=+0} = U\int_{-\infty}^{\infty} d\lambda\, f(\lambda,y)\, e^{i\lambda t}$$

$$\alpha_0(t,y,+0) = \int_{-\infty}^{\infty} d\lambda\, f(\lambda,y)\, e^{i\lambda t}$$

or

$$= 2\int_{0}^{\infty} \left[f_0(\lambda,y)\cos\lambda t + f_1(\lambda,y)\sin\lambda t \right] d\lambda \qquad (2.18)$$

From the theory of complex Fourier transform,

$$f(\lambda,y) = \frac{1}{2\pi}\int_{-\infty}^{\infty} \alpha(t,y)\, e^{-i\lambda t}\, dt \qquad (2.19)$$

This means, that if we choose the source distribution f (λ,y) to be the Fourier transform of the distribution of the angle of attack, the potential ϕ_0 will represent the flow about the wing automatically. Since the angle of attack is zero ahead of the wing, it can be shown easily that equation (2.15) satisfies the second boundary condition of equation (2.12).

2.4 Supersonic Flow about a Lifting Surface

By means of the same argument as in the last section, we can formulate the potential for a doublet sheet of strength

$Re \quad G(\lambda,\eta)\ e^{i\lambda t}$ from equation (2.6).

$$\phi_1(t,y,z) = Re\ \frac{-iU}{4}\int_{-\infty}^{\infty} d\eta \int_{0}^{\infty} d\lambda\ \lambda\ G(\lambda,\eta)\ e^{i\lambda t} H_1^{(2)}(\lambda r).\frac{z}{r} \tag{2.20}$$

where a constant, free stream velocity U is introduced. In order to simplify the later development, we further introduce

$$g(\lambda,\eta) = \frac{i\lambda\ G(\lambda,\eta)}{8m'} = g_0(\lambda,\eta) - i\,g_1(\lambda,\eta) \tag{2.21}$$

where with equation (2.7)

$$g_0(\lambda,\eta) = \frac{\lambda\ G_1(\lambda,\eta)}{8m'} \qquad \text{(even)}$$

$$g_1(\lambda,\eta) = \frac{\lambda\ G_0(\lambda,\eta)}{8m'} \qquad \text{(odd)} \tag{2.22}$$

Then equation (2.20) can be written

$$\phi_1(t,y,z) = Re\left\{-2m'U\int_{-\infty}^{\infty} d\eta \int_{0}^{\infty} d\lambda\ g(\lambda,\eta)\ e^{i\lambda t} H_1^{(2)}(\lambda r).\frac{z}{r}\right\} \tag{2.23}$$

We can write the above equation entirely in the complex form

$$\phi_1(t,y,z) = -m'U\int_{-\infty}^{\infty}d\eta\int_{-\infty}^{\infty}d\lambda\, g(\lambda,\eta)\, e^{i\lambda t}H_1^{(2)}(\lambda r)\cdot\frac{z}{r} \tag{2.24}$$

if the path of λ is restricted to be chosen below $\lambda=0$ in the λ-complex plane. This is necessary because

$$\overline{g(-\lambda,\eta)} = g_0(\lambda,\eta) + i\,g_1(\lambda,\eta) = g(\lambda,\eta)$$

$$H_1^{(2)}(-\lambda r) = H_1^{(2)}(\lambda r e^{-i\pi}) = \overline{H_1^{(2)}(\lambda r)} \tag{2.25}$$

On the other hand, we cannot choose the path of λ with Re $\lambda > 0$ in order to detour $\lambda=0$. In that case,

$$H_1^{(2)}(-\lambda r) = H_1^{(2)}(\lambda r e^{i\pi}) = -H_1^{(2)}(\lambda r) - 2J_1(\lambda r) \neq \overline{H_1^{(2)}(\lambda r)}$$

it is impossible to reduce back to the original equation (2.23).

In order to find out whether equation (2.24) for the doublet sheet satisfies all the boundary conditions of the wing or not, we first differentiate it with respect to t.

$$\frac{\partial\phi_1}{\partial t} = m'\frac{\partial\phi_1}{\partial x} = m'u = -m'Ui\int_{-\infty}^{\infty}d\eta\int_{-\infty}^{\infty}\lambda\, d\lambda\, g(\lambda,\eta)\, e^{i\lambda t}H_1^{(2)}(\lambda r)\cdot\frac{z}{r} \tag{2.26}$$

The above equation is identical in form with equation (2.16) if we replace f (λ, η) by $\frac{m'}{2}$ g (λ, η). Therefore, with the same technique, we can show that as z $\longrightarrow$ 0, $\eta \rightarrow$ y

$$\left(\frac{\partial \phi_1}{\partial t}\right)_{z=+0} = \frac{-m'U}{2} \int_{-\infty}^{\infty} d\lambda \; e^{i\lambda t} g(\lambda, y) \tag{2.27}$$

Now in the linearized theory, the pressure coefficient on the wing surface is

$$C_p(t, y, +0) = \frac{-2u}{U} = \frac{-2}{Um'} \left(\frac{\partial \phi_1}{\partial t}\right)_{z=+0} \tag{2.28}$$

Thus with equation (2.27)

$$C_p(t, y, +0) = \int_{-\infty}^{\infty} d\lambda e^{i\lambda t} g(\lambda, y) \tag{2.29}$$

With the Fourier transform, we can find

$$g(\lambda, y) = \frac{1}{2\pi} \int_{-\infty}^{\infty} dt \; e^{i\lambda t} \; C_p(t, y, +0) \tag{2.30}$$

Therefore, if the pressure distribution along the wing chord is given, the doublet distribution function g (λ, y) of frequency $\frac{\lambda}{2\pi}$ can be obtained with equation (2.30). g (λ, y) is independent of the pressure distribution of the neighboring chord. Furthermore if $\lambda \to 0$ in equation (2.30), we have

$$g(o,y) = \frac{1}{2\pi}\int_{-\infty}^{\infty} dt \;\; C_p(t, y, +o) \tag{2.31}$$

On the right side, $\int_{-\infty}^{\infty} dt \;\; C_p(t,y,+o)$ is equal to one-half of the lift coefficient distribution, $-\frac{1}{2}\left(\frac{\partial C_l}{\partial y}\right)$ at y. Thus, g(0, y) is equivalent to $-\frac{1}{4\pi}\left(\frac{\partial C_l}{\partial y}\right)$ at y which has a physical meaning.

Unfortunately, the equation (2.23) of doublet sheet potential satisfies one of the boundary conditions on the wing, but does not satisfy the other required boundary condition, that the potential and its derivatives must be zero far ahead of the body. In other words, the correct potential must be zero as $t \to -\infty$. Let us investigate the potential of the doublet sheet at large $\pm$ t.

Introduce $\nu = \lambda t$ into equation (2.23)

$$\phi_1(t,y,z) = Re\left\{-2m'U\int_{-\infty}^{\infty} d\eta \int_{-\infty}^{\infty} \frac{d\nu}{t}\; g\left(\frac{\nu}{t}, \eta\right) e^{i\nu} H_1^{(2)}\left(\frac{\nu r}{t}\right)\cdot \frac{z}{r}\right.$$

(2.32)

For very large t we can write $H_1^{(2)}\left(\frac{\nu r}{t}\right) \cong \frac{2it}{\pi \nu r}$

and

$$g\left(\frac{\nu}{t}, \eta\right) = g(0,\eta)$$

$$\lim_{t \to \pm\infty} \phi_1(t,y,z) = \lim_{t \to \pm\infty} Re\left\{\frac{-4m'Ui}{\pi}\int_{-\infty}^{\infty}\frac{z}{r^2}\,d\eta\, g(0,\eta)\int_0^{\infty}\frac{e^{i\nu}}{\nu}\,d\nu\right.$$

$$= \lim_{t \to \pm\infty}\left\{\frac{4m'U}{\pi}\int_{-\infty}^{\infty}\frac{z}{r^2}\,d\eta\, g(0,\eta)\int_0^{\infty}\frac{\sin\nu}{\nu}\,d\nu\right.$$

$$\phi_1(\pm\infty, y, z) = \chi^* = \pm 2m'U\int_{-\infty}^{\infty}\frac{z}{r^2}\,d\eta\, g(0,\eta) \tag{2.33}$$

where the negative sign corresponds to $t = -\infty$ and positive sign corresponds to $t = +\infty$. $\chi^*(y,z)$ being independent of t satisfies the Laplace equation $\frac{\partial^2\chi^*}{\partial x^2} + \frac{\partial^2\chi^*}{\partial y^2} = 0$, and can be added to ϕ, the doublet sheet potential, without an effect on the pressure distribution. It should be noted that the value of potential function as $t \longrightarrow +\infty$ is $2\chi^*$. Hence χ^* may be interpreted physically as the potential function of the downwash in the Trefftz plane.

Thus, from equations (2.24) and (2.33) the complete solution of our problem on supersonic wing lift is

$$\phi(t,y,z) = \phi_1 + \chi^* = m'U\int_{-\infty}^{\infty}\frac{z}{r^2}\,d\eta\left\{2g(0,\eta) - \int_{-\infty}^{\infty} r\,d\lambda\, g(\lambda,\eta)\, e^{i\lambda t} H_1^{(2)}(\lambda r)\right\} \tag{2.34}$$

In the case that C_p is given, the above equation can be written with equation (2.30) and (2.31),

$$\phi(t,y,z) = \frac{m'U}{2\pi}\int_{-\infty}^{\infty}\frac{z}{r^2}d\eta\int_{-\infty}^{\infty}d\tau\, C_p(\tau,\eta,+0)\left\{2-\int_{-\infty}^{\infty}rd\lambda\, e^{i\lambda(t-\tau)}H_1^{(2)}(\lambda r)\right\} \tag{2.35}$$

If we let $\lambda r = v$, we have

$$\phi(t,y,z) = \frac{m'U}{2\pi}\int_{-\infty}^{\infty}\frac{z}{r^2}d\eta\int_{-\infty}^{\infty}d\tau\, C_p(\tau,\eta,+0)\left\{2-\int_{-\infty}^{\infty}dv\, e^{iv\left(\frac{t-\tau}{r}\right)}H_1^{(2)}(v)\right\} \tag{2.36}$$

With reference 19 p. 405, we can evaluate the last integral in the bracket

$$2-\int_{-\infty}^{\infty}dv\, e^{iv\left(\frac{t-\tau}{r}\right)}H_1^{(2)}(v) = \begin{cases} 0 & \left(\frac{t-\tau}{r}\le 1\right) \\ \dfrac{4}{\sqrt{1-\left(\frac{r}{t-\tau}\right)^2}} & \left(\frac{t-\tau}{r}>1\right) \end{cases} \tag{2.37}$$

Thus, if we take the vertex of the foremost Mach Cone as origin, we can write

$$\phi(t,y,z) = \frac{2m'U}{\pi}\int_{-\infty}^{\infty}\frac{z}{r^2}d\eta\int_{-\infty}^{t-\tau}d\tau\,\frac{(t-\tau)\,C_p(\tau,\eta,+0)}{\sqrt{(t-\tau)^2-r^2}} \tag{2.38}$$

which is the equation of the potential in terms of the pressure coefficient on the wing. C_p is zero outside the wing. Since the radical must be positive, ϕ is zero outside the foremost Mach cone, as predicated by other theories.

III. Aerodynamic Behavior of Symmetrical Flat Bodies in Supersonic Flow.

As the disturbance potential for the symmetrical flat body in supersonic flow has been given in equation (2.15b), with the Fourier integral method, the present section will show the expression for the pressure coefficient and wave drag of various types of wing planforms and airfoil sections.

3.1 Derivation of the Expression of Wave Drag of a Wing.

To the order of approximation of the linearized theory, the increment of pressure Δp anywhere within the disturbance area is

$$\Delta p = p - p_o = -\rho_o U u = -\rho_o U \frac{\partial \phi_o}{\partial x} = -\frac{\rho_o U}{m'} \frac{\partial \phi_o}{\partial t} \tag{3.1}$$

where the relations $x = (M^2 - 1)^{\frac{1}{2}} t = m't$, and $u = \frac{\partial \phi_o}{\partial x}$ are used,

p is the local pressure at the point (x, y, $\pm$ z) and p_o, ρ_o are the free stream pressure and density respectively.

To find $\frac{\partial \phi_o}{\partial t}$, we can differentiate equation (2.15b) as

$$\frac{u}{m'} = \frac{\partial \phi_o}{\partial t} = \frac{U}{2} \int_{-\infty}^{\infty} d\eta \int_{-\infty}^{\infty} \lambda \, d\lambda \, f(\lambda, \eta) \, e^{i\lambda t} H_o^{(2)}(\lambda r) \tag{3.2}$$

where $\frac{\partial \phi_o}{\partial t}$ is an even function with respect to z.

Substituting equation (3.2) into equation (3.1), we find

$$\Delta p(x, y, z) = \frac{\rho_o U^2}{2m'} \int_{-\infty}^{\infty} d\eta \int_{-\infty}^{\infty} \lambda \, d\lambda \, f(\lambda, \eta) \, e^{i\lambda t} H_o^{(2)}(\lambda r) \tag{3.3}$$

If we want the pressure increment on the wing surface which is located equivalently at z = + 0, we have $r \longrightarrow |y-\eta|$ and

$$\Delta p(t,y,\pm 0) = \frac{\rho_0 U^2}{2m'} \int_{-\infty}^{\infty} d\eta \int_{-\infty}^{\infty} \lambda\, d\lambda\, f(\lambda,\eta)\, e^{i\lambda t} H_0^{(2)}(\lambda|y-\eta|) \tag{3.4}$$

If we are interested in the wave drag distribution along the span, $\frac{\partial D}{\partial y}$, we must sum up all the horizontal components of the pressure increment along x or t direction on both the top and bottom surfaces over a unit span width. Mathematically

$$\left(\frac{\partial D}{\partial y}\right)_y = 2 \int_{-\infty}^{\infty} \Delta p \cdot \alpha_0\, dx \tag{3.5}$$

where α_0 is the surface slope of the airfoil along the line of constant y as given in equation (2.18). With the expression of α_0 (t, y, +0) and Δp (t, y, 0) in equation (3.4), we can find the drag distribution per unit span as

$$\frac{\partial D}{\partial y} = \rho_0 U^2 \int_{-\infty}^{\infty} d\eta \int_{-\infty}^{\infty} \lambda\, d\lambda\, H_0^{(2)}(\lambda|y-\eta|) \cdot f(\lambda,\eta) \int_{-\infty}^{\infty} dt \int_{-\infty}^{\infty} d\lambda'\, e^{i(\lambda+\lambda')t} \cdot f(\lambda', y) \tag{3.6}$$

where λ' and y correspond to α_0. To evaluate the last double integral, let us write $\lambda' = -\lambda''$ and the double integral can be written as

$$\int_{-\infty}^{\infty} dt \int_{-\infty}^{\infty} d\lambda' \, e^{i(\lambda+\lambda')t} \cdot f(\lambda', y) = \int_{-\infty}^{\infty} dt \int_{+\infty}^{-\infty} (-d\lambda'') \, e^{i(\lambda-\lambda'')t} \cdot f(-\lambda'', y)$$

$$= \int_{-\infty}^{\infty} dt \int_{-\infty}^{\infty} d\lambda'' \, e^{i(\lambda-\lambda'')t} \cdot \overline{f(\lambda'', y)} \tag{3.7}$$

where

$$f(-\lambda'', y) = f_0(-\lambda'', y) + i f_1(-\lambda'', y) = f_0(\lambda'', y) - i f_1(\lambda'', y)$$

$$= \overline{f(\lambda'', y)}$$

is introduced because of f_0 being even, f_1, being odd. From the complex Fourier integral theorem,

$$2\pi \, \overline{f(\lambda, y)} = \int_{-\infty}^{\infty} dt \int_{-\infty}^{\infty} d\lambda'' \, e^{i(\lambda-\lambda'')t} \cdot \overline{f(\lambda'', y)} \tag{3.8}$$

if the Lebesgue integral $\int_{-\infty}^{\infty} d\lambda'' \, |f(\lambda'', y)| < \infty$ exists or if $f(\lambda'', y)$ is of bounded variation, in the neighborhood of $\lambda = \lambda''$

(See theorem 23 reference 18, p. 42).

Substituting equation (3.8) into equation (3.6) we have

$$\left(\frac{\partial D}{\partial y}\right)_y = 2\pi\rho_0 U^2 \int_{-\infty}^{\infty} d\eta \int_{-\infty}^{\infty} \lambda d\lambda\, H_0^{(2)}(\lambda|y-\eta|)\cdot f(\lambda,\eta)\cdot \overline{f(\lambda,y)}$$

$$= 2\pi\rho_0 U^2 \int_{-\infty}^{\infty} d\eta \int_{-\infty}^{\infty} \lambda d\lambda \left\{ H_0^{(2)}(\lambda|y-\eta|) f(\lambda,\eta)\overline{f(\lambda,y)} + \overline{H_0^{(2)}(\lambda|y-\eta|)}\cdot\overline{f(\lambda,\eta)} f(\lambda,y) \right\}$$

$$= 2\pi\rho_0 U^2 \int_{-\infty}^{\infty} d\eta \int_{-\infty}^{\infty} \lambda d\lambda \left\{ J_0(\lambda|y-\eta|)\left[f_0(\lambda,\eta)f_0(\lambda,y) + f_1(\lambda,\eta)f_1(\lambda,y)\right] \right.$$

$$\left. + Y_0(\lambda|y-\eta|)\left[f_1(\lambda,\eta)f_0(\lambda,y) - f_0(\lambda,\eta)f_1(\lambda,y)\right] \right\} \qquad (3.9)$$

where a few relations are used

$$H_0^{(2)}(-\lambda|y-\eta|) = \overline{H_0^{(2)}(\lambda|y-\eta|)} = J_0(\lambda|y-\eta|) - i\,Y_0(\lambda|y-\eta|)$$

$$f(-\lambda,\eta)\cdot\overline{f(-\lambda,y)} = \overline{f(\lambda,\eta)}\cdot f(\lambda,y)$$

so that the integration limit changes from 0 to ∞ instead of $-\infty$ to $+\infty$. The imaginary part automatically cancels out.

Now if we want D, the wave drag of the whole wing system, we can integrate equation (3.9) with respect to y,

$$D = \int_{-\infty}^{\infty} \left(\frac{\partial D}{\partial y}\right) dy = 2\pi\rho_0 U^2 \int_{-\infty}^{\infty} dy \int_{-\infty}^{\infty} d\eta \int_{-\infty}^{\infty} \lambda\, d\lambda\, H_0^{(2)}(\lambda|y-\eta|)\, f(\lambda,\eta)\overline{f(\lambda,y)}$$

$$= 4\pi\rho_0 U^2 \int_{-\infty}^{\infty} dy \int_{-\infty}^{\infty} d\eta \int_{0}^{\infty} \lambda\, d\lambda \left\{ J_0(\lambda|y-\eta|)\left[f_0(\lambda,\eta) f_0(\lambda,y) + f_1(\lambda,\eta) f_1(\lambda,y)\right] \right.$$

$$\left. + Y_0(\lambda|y-\eta|)\left[f_1(\lambda,\eta) f_0(\lambda,y) - f_0(\lambda,\eta) f_1(\lambda,y)\right] \right\}$$

(3.10)

Now the wave drag D being independent of y and η should be independent of the order of integration or of the interchange of y with η .

In carrying out such an interchange we have

$$D' = 4\pi\rho_0 U^2 \int_{-\infty}^{\infty} d\eta \int_{-\infty}^{\infty} dy \int_{0}^{\infty} \lambda\, d\lambda \left\{ J_0(\lambda|\eta-y|)\left[f_0(\lambda,y) f_0(\lambda,\eta) + f_1(\lambda,y) f_1(\lambda,\eta)\right] \right.$$

$$\left. + Y_0(\lambda|\eta-y|)\left[f_1(\lambda,y) f_0(\lambda,\eta) - f_0(\lambda,y) f_1(\lambda,\eta)\right] \right\}$$

This shows that the necessary condition D = D′ is

$$\int_{-\infty}^{\infty} d\eta \int_{-\infty}^{\infty} dy \int_{0}^{\infty} \lambda\, d\lambda \left\{ Y_0(\lambda|\eta-y|)\left[f_1(\lambda,y) f_0(\lambda,\eta) - f_0(\lambda,y) f_1(\lambda,\eta)\right] \right\} = 0$$

(3.11)

This is one of the important relations that has been developed by Professor von Kármán. There is another way of evaluating the wave drag as pointed out by Professor von Kármán. The total momentum transfer through a cylindrical surface of very large radius R which contains the wing in the flight direction must be equal to the wave drag, by means of Newton's laws. Thus

$$D = -\rho_o \int_{-\infty}^{\infty} dt \int_{0}^{2\pi} R\, d\theta \cdot \frac{\partial \phi}{\partial r} \cdot \frac{\partial \phi}{\partial t} \tag{3.12}$$

which is the same as equation (3.10). Applying equation (3.11) we can write equation (3.10) as

$$D = 4\pi \rho_o U^2 \int_{-\infty}^{\infty} dy \int_{-\infty}^{\infty} d\eta \int_{0}^{\infty} \lambda\, d\lambda\, J_o(\lambda|y-\eta|)\left[f_o(\lambda,\eta) f_o(\lambda,y) + f_1(\lambda,\eta) f_1(\lambda,y)\right] \tag{3.13}$$

In case of swept-back wing which is symmetrical with respect to the (x, z) plane, $f_o(\lambda, y)$ and $f_1(\lambda, y)$ are even functions with respect to y. To take care of this point, we can write

$$D = 4\pi \rho_o U^2 \int_{-\infty}^{\infty} dy \int_{-\infty}^{\infty} d\eta \int_{0}^{\infty} \lambda\, d\lambda\, J_o(\lambda|y-\eta|)\left[f_o(\lambda,|\eta|) f_o(\lambda,|y|) + f(\lambda,\eta) f_1(\lambda,|y|)\right]$$

$$= 4\pi \rho_o U^2 \int_{-\infty}^{\infty} dy \int_{0}^{\infty} d\eta \int_{0}^{\infty} \lambda\, d\lambda \left[J_o(\lambda|y-\eta|) + J_o(\lambda|y+\eta|)\right]\left[f_o(\lambda,\eta) f_o(\lambda,|y|) + f_1(\lambda,\eta) f_1(\lambda,|y|)\right]$$

$$= 8\pi \rho_o U^2 \int_{0}^{\infty} dy \int_{0}^{\infty} d\eta \int_{0}^{\infty} \lambda\, d\lambda \left[J_o(\lambda|y-\eta|) + J_o(\lambda|y+\eta|)\right]\left[f_o(\lambda,\eta) f_o(\lambda,y) + f_1(\lambda,\eta) f_1(\lambda,y)\right] \tag{3.14}$$

where the limits of η and y change as shown. Equation (3.14) will be used in the next section very often. If the span is finite (say that b = semispan) and the airfoil sections are similar everywhere, we can write equation (3.14)

$$D = 8\pi\rho_0 U^2 \int_0^b dy \int_0^b d\eta \int_0^\infty \lambda d\lambda \left[J_0(\lambda|y-\eta|) + J_0(\lambda|y+\eta|) \right] \left[f_0(\lambda,\eta) f_0(\lambda,y) + f_1(\lambda,\eta) f_1(\lambda,y) \right] \tag{3.15}$$

3.2 Wave Drag of a Tapered Swept-Back Wing

If we take the double-wedge profile as the airfoil section of the wing as shown in Appendix A, and introduce Equation (A-8) into equation (3.15), we have

$$D = 8\pi\rho_0 U^2 \int_0^b dy \int_0^b d\eta \int_0^\infty \lambda d\lambda \left\{ J_0(\lambda\{y-\eta\}) + J_0(\lambda\{y+\eta\}) \right\} \times$$

$$\frac{\alpha'^2}{\pi^2\lambda^2} (1-\cos\lambda a'_y)(1-\cos\lambda a'_\eta) \cos\lambda\beta(y-\eta)$$

$$= \frac{8\rho_0 U^2 \alpha'^2_0}{\pi} \int_0^b dy \int_0^b d\eta \int_0^\infty \frac{d\lambda}{\lambda} \left\{ J_0(\lambda\{y-\eta\}) + J_0(\lambda\{y+\eta\}) \right\} \times$$

$$(1-\cos\lambda a'_y)(1-\cos\lambda a'_\eta) \cos\lambda\beta(y-\eta) \tag{3.16}$$

Define

$$b' = \frac{b}{a_o'} \qquad y' = \frac{y}{a_o'} \qquad \eta' = \frac{\eta}{a_o'} \qquad v' = \frac{v}{m'}$$

$$a_y' = a_o' (1 - v'y')$$

$$a_\eta' = a_o' (1 - v'\eta') \tag{3.17}$$

For details of the notation refer to Fig. 1 and Appendix C.

We can write the wave drag equation in another form

$$\frac{\pi D}{\beta \rho_o U^2 \alpha_o'^2 a_o'^2} = \int_0^{b'} dy' \int_0^{b'} d\eta' \int_0^{\infty} \frac{d\lambda}{\lambda} \left\{ J_o[(\eta'-y')\lambda a_o'] + J_o[(\eta'+y')\lambda a_o'] \right\} X$$

$$\left\{ -\frac{1}{4}\left[1 - \cos\lambda a_o'\{2+\beta(\eta'-y') - v'(\eta'+y')\}\right] - \frac{1}{4}\left[1 - \cos\lambda a_o'\{2-\beta(\eta'-y') - v'(\eta'+y')\}\right] \right.$$

$$-\frac{1}{4}\left[1 - \cos\lambda a_o'(\beta+v')(\eta'-y')\right] - \frac{1}{4}\left[1 - \cos\{\lambda a_o'(\beta-v')(\eta'-y')\}\right]$$

$$+\frac{1}{2}\left[1 - \cos\lambda a_o'\{1+\beta(\eta'-y') - v'y'\}\right] + \frac{1}{2}\left[1 - \cos\lambda a_o'\{1-\beta(\eta'-y') - v'y'\}\right]$$

$$+\frac{1}{2}\left[1 - \cos\lambda a_o'\{1+\beta(\eta'-y') - v'\eta'\}\right] + \frac{1}{2}\left[1 - \cos\lambda a_o'\{1-\beta(\eta'-y') - v'\eta'\}\right] \tag{3.18}$$

$$\left. - \left[1 - \cos\beta\lambda a_o'(\eta'-y')\right] \right\}$$

With the known infinite integrals of Bessel functions as shown in Appendix B, we can carry out the integration in equation (3.18),

$$\frac{\pi D}{8P_0U^2\alpha_0'^2a_0'^2} = \int_0^{b'} dy' \int_0^{b'} d\eta' \left\{ -\frac{1}{4}\cosh^{-1}\frac{2+\beta(\eta'-y')-\nu'(\eta'+y')}{\eta'-y'} - \frac{1}{4}\cosh^{-1}\frac{2+\beta(\eta'-y')-\nu'(\eta'+y')}{\eta'+y'} \right.$$

$$-\frac{1}{4}\cosh^{-1}\frac{2-\beta(\eta'-y')-\nu'(\eta'+y')}{\eta'-y'} - \frac{1}{4}\cosh^{-1}\frac{2-\beta(\eta'-y')-\nu'(\eta'+y')}{\eta'+y'}$$

$$-\frac{1}{4}\cosh^{-1}\frac{(\beta+\nu')(\eta'-y')}{\eta'+y'} - \frac{1}{4}\cosh^{-1}(\beta+\nu') - \frac{1}{4}\cosh^{-1}(\beta-\nu')$$

$$-\frac{1}{4}\cosh^{-1}\frac{(\beta-\nu')(\eta'-y')}{\eta'+y'} + \frac{1}{2}\cosh^{-1}\frac{1+\beta(\eta'-y')-\nu'y'}{\eta'-y'} + \frac{1}{2}\cosh^{-1}\frac{1+\beta(\eta'-y')-\nu'y'}{\eta'+y'}$$

$$+\frac{1}{2}\cosh^{-1}\frac{1-\beta(\eta'-y')-\nu'y'}{\eta'+y'} + \frac{1}{2}\cosh^{-1}\frac{1-\beta(\eta'-y')-\nu'y'}{\eta'-y'} + \frac{1}{2}\cosh^{-1}\frac{1+\beta(\eta'-y')-\nu'\eta'}{\eta'-y'}$$

$$+\frac{1}{2}\cosh^{-1}\frac{1+\beta(\eta'-y')-\nu'\eta'}{\eta'+y'} + \frac{1}{2}\cosh^{-1}\frac{1-\beta(\eta'-y')-\nu'\eta'}{\eta'-y'} + \frac{1}{2}\cosh^{-1}\frac{1-\beta(\eta'-y')-\nu'\eta'}{\eta'+y'}$$

$$\left. -\cosh^{-1}\frac{\beta(\eta'-y')}{\eta'+y'} - \cosh^{-1}\beta \right\} \qquad (3.19)$$

In all $\cosh^{-1}(A)$ terms, A must be positive. In order to carry out the integration, a transformation of the coordinate system may be introduced:

Let $u' = \eta' + y'$, $v' = \eta' - y'$. Then

$$dy'd\eta' = \frac{\partial(y', \eta')}{\partial(u', v')} du'dv' = \frac{1}{2} du'dv'$$

$$y'=0 , \eta'=0 \longrightarrow u'=0 , v'=0$$

$$y'=0 , \eta'=b' \longrightarrow u'=b' , v'=b'$$

$$y'=b' , \eta'=0 \longrightarrow u'=b' , v'=-b'$$

$$y'=b' , \eta'=b' \longrightarrow u'=2b' , v'=0$$

With this transformation, the square domain in (y', η') plane will transform to a diamond shaped domain (of twice the area) in (u', v') plane.

$$\frac{\pi D}{8\rho_o U_o^2 \alpha_o'^2 a_o'^2} = -b'^2\left\{\frac{1}{4}\cosh^{-1}(\beta+\nu') + \frac{1}{4}\cosh^{-1}(\beta-\nu') + \cosh^{-1}\beta\right\}$$

$$+\int_0^{b'}du'\int_0^{u'}dv'\left\{\left[-\frac{1}{4}\cosh^{-1}\left(\frac{2-\nu'u'}{v'}+\beta\right)-\frac{1}{4}\cosh^{-1}\left(\frac{2+\beta v'}{u'}-\nu'\right)-\frac{1}{4}\cosh^{-1}\left(\frac{2-\nu'u'}{v'}-\beta\right)-\frac{1}{4}\cosh^{-1}\left(\frac{2-\beta v'}{u'}-\nu'\right)\right.\right.$$

$$\left.-\frac{1}{4}\cosh^{-1}\frac{(\beta+\nu')v'}{u'}-\frac{1}{4}\cosh^{-1}\frac{(\beta-\nu')v'}{u'}\right]+\left[-\frac{1}{4}\cosh^{-1}\left(\frac{2-2\nu'b'+\nu'u'}{v'}+\beta\right)-\frac{1}{4}\cosh^{-1}\left(\frac{2+\beta v'}{2b'-u'}-\nu'\right)\right.$$

$$\left.-\frac{1}{4}\cosh^{-1}\left(\frac{2-2\nu'b'+\nu'u'}{v'}-\beta\right)-\frac{1}{4}\cosh^{-1}\left(\frac{2-\beta v'}{2b'-u'}-\nu'\right)-\frac{1}{4}\cosh^{-1}\frac{(\beta+\nu')v'}{2b'-u'}-\frac{1}{4}\cosh^{-1}\frac{(\beta-\nu')v'}{2b'-u'}\right]$$

$$+\frac{1}{2}\left[\cosh^{-1}\left(\frac{2-\nu'u'}{2v'}+\beta+\frac{\nu'}{2}\right)+\cosh^{-1}\left(\frac{2+\{2\beta+\nu'\}v'}{2u'}-\frac{\nu'}{2}\right)+\cosh^{-1}\left(\frac{2-\nu'u'}{2v'}-\beta+\frac{\nu'}{2}\right)+\cosh^{-1}\left(\frac{2+\{2\beta-\nu'\}v'}{2u'}-\frac{\nu'}{2}\right)\right.$$

$$\left.+\cosh^{-1}\left(\frac{2-\nu'u'}{2v'}+\beta-\frac{\nu'}{2}\right)+\cosh^{-1}\left(\frac{2+\{2\beta-\nu'\}v'}{2u'}-\frac{\nu'}{2}\right)+\cosh^{-1}\left(\frac{2-\nu'u'}{2v'}-\beta-\frac{\nu'}{2}\right)+\cosh^{-1}\left(\frac{2-\{2\beta+\nu'\}v'}{2u'}-\frac{\nu'}{2}\right)\right]$$

$$+\frac{1}{2}\left[\cosh^{-1}\left(\frac{2-2\nu'b'+\nu'u'}{2v'}+\beta+\frac{\nu'}{2}\right)+\cosh^{-1}\left(\frac{2+\{2\beta+\nu'\}v'}{2\{2b'-u'\}}-\frac{\nu'}{2}\right)\right.$$

$$\left.+\cosh^{-1}\left(\frac{2-2\nu'b'+\nu'u'}{2v'}-\beta+\frac{\nu'}{2}\right)+\cosh^{-1}\left(\frac{2-\{2\beta-\nu'\}v'}{2\{2b'-u'\}}-\frac{\nu'}{2}\right)\right.$$

$$\left.+\cosh^{-1}\left(\frac{2-2\nu'b'+\nu'u'}{2v'}+\beta-\frac{\nu'}{2}\right)+\cosh^{-1}\left(\frac{2+\{2\beta-\nu'\}v'}{2\{2b'-u'\}}-\frac{\nu'}{2}\right)+\cosh^{-1}\left(\frac{2-2\nu'b'+\nu'u'}{2v'}-\beta-\frac{\nu'}{2}\right)\right.$$

$$\left.+\cosh^{-1}\left(\frac{2-\{2\beta+\nu'\}v'}{2\{2b'-u'\}}-\frac{\nu'}{2}\right)\right]+\left[-\cosh^{-1}\frac{\beta v'}{u'}-\cosh^{-1}\frac{\beta v'}{2b'-u'}\right]\Bigg\} \qquad (3.20)$$

The details of the integration are too complicated to be given here. The result can be summarized in equation (3.21).

$$\frac{\pi}{2} b'(1+\sigma)\frac{C_D}{C_{D_0}} = b'^2\left(4\cosh^{-1}\frac{\sigma}{2b'} - \cosh^{-1}\frac{\sigma}{b'}\right) - b'^2\frac{\beta_0}{2(\beta_0^2-1)^{1/2}}\cosh^{-1}\left|\frac{\beta_0^2+1}{2\beta_0}\right|^{a} - b'^2\frac{\beta_1}{2(\beta_1^2-1)^{1/2}}\cosh^{-1}\left|\frac{\beta_1^2+1}{2\beta_1}\right|^{b} - b'^2\frac{2\beta}{(\beta^2-1)^{1/2}}\cosh^{-1}\left|\frac{\beta^2+1}{2\beta}\right|^{c}$$

$$+\left\{\begin{array}{l}\dfrac{(1+\beta b')^2}{2\beta(1-\beta_0^2)^{1/2}}\left\{-\sin^{-1}\dfrac{\sigma\beta_0+b'}{1+\beta b'}+\sin^{-1}\left[\beta_0+\dfrac{(1-\beta_0^2)b'}{2(1+\beta b')}\right]\right\}+\dfrac{(\sigma+2\beta_0 b')^2}{2(\beta_0+\beta)(1-\beta_0^2)^{1/2}}\left\{\sin^{-1}\dfrac{\sigma\beta_0+2b'}{\sigma+2\beta_0 b'}-\sin^{-1}\left[\beta_0+\dfrac{(1-\beta_0^2)b'}{\sigma+2\beta_0 b'}\right]\right\}\\ \dfrac{(1+\beta b')^2}{2\beta(\beta_0^2-1)^{1/2}}\left\{\cosh^{-1}\left|\dfrac{\sigma\beta_0+b'}{1+\beta b'}\right|-\cosh^{-1}\left|\beta_0+\dfrac{(1-\beta_0^2)b'}{2(1+\beta b')}\right|\right\}+\dfrac{(\sigma+2\beta_0 b')^2}{2(\beta_0+\beta)(\beta_0^2-1)^{1/2}}\left\{-\cosh^{-1}\left|\dfrac{\sigma\beta_0+2b'}{\sigma+2\beta_0 b'}\right|+\cosh^{-1}\left|\beta_0+\dfrac{(1-\beta_0^2)b'}{\sigma+2\beta_0 b'}\right|\right\}\end{array}\right\}\ \text{A}$$

$$+\left\{\begin{array}{l}\dfrac{(1-\beta b')^2}{2\beta(1-\beta_1^2)^{1/2}}\left\{-\sin^{-1}\dfrac{\sigma\beta_1-b'}{1-\beta b'}+\sin^{-1}\left[\beta_1-\dfrac{(1-\beta_1^2)b'}{2(1-\beta b')}\right]\right\}+\dfrac{(\sigma-2\beta_1 b')^2}{2(\beta_1+\beta)(1-\beta_1^2)^{1/2}}\left\{\sin^{-1}\dfrac{\sigma\beta_1-2b'}{\sigma-2\beta_1 b'}-\sin^{-1}\left[\beta_1-\dfrac{(1-\beta_1^2)b'}{\sigma-2\beta b'}\right]\right\}\\ \dfrac{(1-\beta b')^2}{2\beta(\beta_1^2-1)^{1/2}}\left\{\cosh^{-1}\left|\dfrac{\sigma\beta_1-b'}{1-\beta b'}\right|-\cosh^{-1}\left|\beta_1-\dfrac{(1-\beta_1^2)b'}{2(1-\beta b')}\right|\right\}+\dfrac{(\sigma-2\beta_1 b')^2}{2(\beta_1+\beta)(\beta_1^2-1)^{1/2}}\left\{-\cosh^{-1}\left|\dfrac{\sigma\beta_1-2b'}{\sigma-2\beta_1 b'}\right|+\cosh^{-1}\left|\beta_1-\dfrac{(1-\beta_1^2)b'}{\sigma-2\beta b'}\right|\right\}\end{array}\right\}\ \text{B}$$

$$+\left\{\begin{array}{l}\dfrac{(\sigma-2\beta b')^2}{2(\beta_0+\beta)(1-\beta^2)^{1/2}}\left\{\sin^{-1}\dfrac{\sigma\beta-2b'}{\sigma-2\beta b'}-\sin^{-1}\left[\beta-\dfrac{(1-\beta^2)b'}{\sigma-2\beta b'}\right]\right\}+\dfrac{(\sigma+2\beta b')^2}{2(\beta_1+\beta)(1-\beta^2)^{1/2}}\left\{\sin^{-1}\dfrac{\sigma\beta+2b'}{\sigma+2\beta b'}-\sin^{-1}\left[\beta+\dfrac{(1-\beta^2)b'}{\sigma+2\beta b'}\right]\right\}\\ \dfrac{(\sigma-2\beta b')^2}{2(\beta_0+\beta)(\beta^2-1)^{1/2}}\left\{-\cosh^{-1}\left|\dfrac{\sigma\beta-2b'}{\sigma-2\beta b'}\right|+\cosh^{-1}\left|\beta-\dfrac{(1-\beta^2)b'}{\sigma-2\beta b'}\right|\right\}+\dfrac{(\sigma+2\beta b')^2}{2(\beta_1+\beta)(\beta^2-1)^{1/2}}\left\{-\cosh^{-1}\left|\dfrac{\sigma\beta+2b'}{\sigma+2\beta b'}\right|+\cosh^{-1}\left|\beta+\dfrac{(1-\beta^2)b'}{\sigma+2\beta b'}\right|\right\}\end{array}\right\}\ \text{C}$$

$$+\left\{\begin{array}{l}\dfrac{1}{2v'(1-\beta_0^2)^{1/2}}\left\{-\sigma^2\sin^{-1}\left[\beta_0-\dfrac{(1-\beta_0^2)b'}{2\sigma}\right]+\sigma^2\sin^{-1}\left[\beta_0-\dfrac{(1-\beta_0^2)b'}{\sigma}\right]-\dfrac{\beta_1}{\beta}\sin^{-1}\left[\beta_0+(1-\beta_0^2)\dfrac{b'}{2}\right]+\dfrac{2\beta}{\beta_0+\beta}\sin^{-1}\left[\beta_0+(1-\beta_0^2)b'\right]-\dfrac{\beta_0(\beta_0-\beta)}{\beta(\beta_0+\beta)}\sin^{-1}\beta_0\right\}\\ \dfrac{1}{2v'(\beta_0^2-1)^{1/2}}\left\{\sigma^2\cosh^{-1}\left|\beta_0-\dfrac{(1-\beta_0^2)b'}{2\sigma}\right|-\sigma^2\cosh^{-1}\left|\beta_0-\dfrac{(1-\beta_0^2)b'}{\sigma}\right|+\dfrac{\beta_1}{\beta}\cosh^{-1}\left|\beta_0+(1-\beta_0^2)\dfrac{b'}{2}\right|-\dfrac{2\beta}{\beta_0+\beta}\cosh^{-1}\left|\beta_0+(1-\beta_0^2)b'\right|+\dfrac{\beta_0(\beta_0-\beta)}{\beta(\beta_0+\beta)}\cosh^{-1}|\beta_0|\right\}\end{array}\right\}\ \text{D}$$

$$+\left\{\begin{array}{l}\dfrac{1}{2v'(1-\beta_1^2)^{1/2}}\left\{\sigma^2\sin^{-1}\left[\beta_1+\dfrac{(1-\beta_1^2)b'}{2\sigma}\right]-\sigma^2\sin^{-1}\left[\beta_1+\dfrac{(1-\beta_1^2)b'}{\sigma}\right]+\dfrac{\beta_0}{\beta}\sin^{-1}\left[\beta_1-(1-\beta_1^2)\dfrac{b'}{2}\right]-\dfrac{2\beta}{(\beta_1+\beta)}\sin^{-1}\left[\beta_1-(1-\beta_1^2)b'\right]+\dfrac{\beta_1(\beta-\beta_1)}{\beta(\beta_1+\beta)}\sin^{-1}\beta_1\right\}\\ \dfrac{1}{2v'(\beta_1^2-1)^{1/2}}\left\{-\sigma^2\cosh^{-1}\left|\beta_1+\dfrac{(1-\beta_1^2)b'}{2\sigma}\right|+\sigma^2\cosh^{-1}\left|\beta_1+\dfrac{(1-\beta_1^2)b'}{\sigma}\right|-\dfrac{\beta_0}{\beta}\cosh^{-1}\left|\beta_1-(1-\beta_1^2)\dfrac{b'}{2}\right|+\dfrac{2\beta}{(\beta_1+\beta)}\cosh^{-1}\left|\beta_1-(1-\beta_1^2)b'\right|-\dfrac{\beta_1(\beta-\beta_1)}{\beta(\beta_1+\beta)}\cosh^{-1}|\beta_1|\right\}\end{array}\right\}\ \text{E}$$

$$+\left\{\begin{array}{l}\dfrac{1}{2v'(1-\beta^2)^{1/2}}\left\{\sigma^2\sin^{-1}\left[\beta-\dfrac{(1-\beta^2)b'}{2\sigma}\right]-\sigma^2\sin^{-1}\left[\beta-\dfrac{(1-\beta^2)b'}{\sigma}\right]+\dfrac{2\beta_1}{\beta_1+\beta}\sin^{-1}\left[\beta+(1-\beta^2)b'\right]-\dfrac{2\beta_0}{\beta_0+\beta}\sin^{-1}\left[\beta+(1-\beta_0^2)b'\right]+\dfrac{4\beta(\beta_0-\beta)}{(\beta_0+\beta)(\beta_1+\beta)}\sin^{-1}\beta\right\}\\ \dfrac{1}{2v'(\beta^2-1)^{1/2}}\left\{-\sigma^2\cosh^{-1}\left|\beta-\dfrac{(1-\beta^2)b'}{2\sigma}\right|+\sigma^2\cosh^{-1}\left|\beta-\dfrac{(1-\beta^2)b'}{\sigma}\right|-\dfrac{2\beta_1}{\beta_1+\beta}\cosh^{-1}\left|\beta+(1-\beta^2)b'\right|+\dfrac{2\beta_0}{\beta_0+\beta}\cosh^{-1}\left|\beta+(1-\beta_0^2)b'\right|-\dfrac{4\beta(\beta_0-\beta)}{(\beta_0+\beta)(\beta_1+\beta)}\cosh^{-1}|\beta|\right\}\end{array}\right\}\ \text{F}$$

(3.21)

where

$\beta_0 = \beta + \nu'$, $\beta_1 = \beta - \nu'$, $\sigma = 1 - \nu' b'$; $\sin^{-1} A = (\text{sign } A)\frac{\pi}{2}$ if $|A| > 1$;

the upper line with $1-\beta^2$ should be used, if $\beta < 1$;

the lower line with $\beta^2 - 1$ should be used, if $\beta > 1$;

the signs of all $\cosh^{-1}$ terms should be reversed if $\beta < -1$;

the above rules should be also applied for β_0 and β_1 .

a, b, c, A, B, C, etc. represent the expressions in the respective brackets.

Therefore the above equation (3.21) covers all cases except a few limiting cases $\beta = \pm 1$, $\beta_0 = \pm 1$, $\beta_1 = \pm 1$, $\nu' = 0$ and $\beta = \infty$ (i.e. $M \to 1$)

These limiting cases will be shown in the next section.

For a given swept-back wing, $\beta_0 > 1, = 1$ or < 1 means the Mach line ahead, on or behind the leading edge respectively. $\beta_1 > 1, = 1$ or < 1 means the Mach line ahead, on or behind the trailing edge. With a fixed taper ratio, the trailing edge may be swept forward. $\beta_1 = -1$ means the swept-forward trailing edge coincides with the Mach line. Similarly β refers to the middle-chord line or the line of the maximum thickness. At all β's $= |1|$, there occurs a discontinuity of the slope of the curve of the wave drag. In other words, β's $= |1|$ curves are the envelopes of cusps of the $\frac{C_D}{C_{D_0}}$ curves at constant β .

To demonstrate the use of these results, the wave drag coefficients of two families of swept-back wings have been calculated as shown in Figs. 2 and 3 with taper ratio $\sigma = 0.2$ and $\sigma = 0.5$ respectively. The essential parameters are $\frac{C_D}{C_{Do}}$, AR $\tan\gamma$ and β. The effect of the Mach number is contained in $\beta = \frac{\tan\gamma}{m'} = \frac{\tan\gamma}{\sqrt{M^2-1}}$ and $C_{D_o} = \frac{4\alpha_o^2}{\sqrt{M^2-1}}$, the two-dimensional wave drag coefficient of Ackert. To use these curves, first we fix the swept-back angle γ and the aspect ratio. Of course, we have to choose $\sigma = 0.2$ or 0.5 in order to use these graphs. Then with a fixed AR $\tan\gamma$, read off $\frac{C_D}{C_{Do}}$ at various β along the fixed abscissa. Replotting $\frac{C_D}{C_{Do}}$ vs β, the example shown in Fig. 4, actually gives a family swept wings of the fixed AR $\tan\gamma$. The curve C_D vs Mach number can be plotted from the relation $M = \sqrt{\left(\frac{\tan\gamma}{\beta}\right)^2 + 1}$. This is not given in this report.

It is very interesting to note that $\left(\frac{C_D}{C_{Do}}\right)_{max}$ occur when the Mach line coincides with the leading edge, $\beta_o = 1$, or the line of maximum thickness $\beta = 1$. In Fig. 2, ($\sigma = 0.2$), $\left(\frac{C_D}{C_{Do}}\right)_{max.}$ occurs at $\beta = 1$ for AR $\tan\gamma > 7.5$ approximately, and at $\beta_o = 1$ for AR $\tan\gamma < 7.5$. In Fig. 3, ($\sigma = 0.5$), $\left(\frac{C_D}{C_{Do}}\right)_{max.}$ occurs always at $\beta_o = 1$ except AR $\tan\gamma < \frac{2}{3}$. Also $\frac{C_D}{C_{D_o}}$ increases monotonically with AR $\tan\gamma$ at $\beta_o = 1$, $\beta = 1$ or $\beta_1 = 1$, but decreases monotonically with AR $\tan\gamma$ for $\beta_1 = -1$.

Fig. 5 shows β corresponding to $\beta_o = 1$ and $\beta_1 = 1$ against AR tan γ . This is needed for locating the cusp of $\frac{C_D}{C_{D_o}}$ vs β as shown in Fig. 4. These curves are obtained from the relations:

$$\beta_1 = \beta \left\{ 1 - \frac{2(1-\sigma)}{(1+\sigma) AR \tan\gamma} \right\}$$

$$\beta_o = \beta \left\{ 1 + \frac{2(1-\sigma)}{(1+\sigma) AR \tan\gamma} \right\}$$

A number of interesting facts can be shown in Figs. 2 and 3.

(a) The lines $\beta_o = 1$, $\beta_1 = 1$ and $\beta_1 = -1$ are the loci of the cusps of the curves, $\frac{C_D}{C_{D_o}}$ vs AR tan γ at various β . Specifically, the line $\beta_o = 1$ is the locus of cusps of those curves with $\beta < 1$, and the lines $\beta_1 = \pm 1$ are the loci of cusps of those curves with $\beta > 1$.

(b) When γ is negative, there are two possible cases: (i) the flow direction is reversed or (ii) the wing is swept forward. In case (i), the curves $\frac{C_D}{C_{D_o}}$ vs $-$ AR tan $|\gamma|$ are actually the mirror images of the curves shown in the graphs, reflected on the vertical axis with the following changes:

$$\beta \longrightarrow -\beta$$

$$\beta_o = 1 \longrightarrow \beta_1 = -1$$

$$\beta_1 = 1 \longrightarrow \beta_o = -1$$

$$\beta_1 = -1 \longrightarrow \beta_o = +1$$

where the old leading edge changes into the new trailing edge and the old trailing edge into the new leading edge, if the flow direction is reversed.

In case (ii), the curves shown can be used with the following changes:

$$\beta \longrightarrow -\beta$$

$$\beta_0 = 1 \longrightarrow \beta_0 = -1$$

$$\beta_1 = 1 \longrightarrow \beta_1 = -1$$

$$\beta_1 = -1 \longrightarrow \beta_1 = 1$$

Therefore, these graphs can be used to find $\frac{C_D}{C_{D_0}}$ at various values of AR tan $|\gamma|$ and $|\beta|$ for the wing swept forward or backward or for the same wing flying forward or backward, as long as the taper ratio is kept constant as specified. Therefore, the wave drag depends only on the absolute values of AR tan γ and β. This confirms the reverse flow theorem in reference 2 and 5.

(c) When $\beta = 0$ $\left(\beta = \frac{\tan\gamma}{\sqrt{M^2-1}}\right)$, there are two possible cases: (i) $M \to \infty$ if $(\gamma) \neq 0$, or (ii) $\gamma = 0$, if $M > 1$. In these graphs, $\beta = 0$ corresponds to $\frac{C_D}{C_{D_0}} = 1$. In other words, the wave drag coefficient is the same as that of the two-dimensional case. Actually, when $M >> 1$, the assumptions of the linearized theory become unreliable. Besides case (i) has no physical reality. In case (ii), $\gamma = 0$ corresponds to AR tan $\gamma = 0$. These graphs can not be used to

determine the wave drag in such a case. The investigation for $\gamma = o$ is rather easy, and is omitted in this paper. Although the line $\frac{C_D}{C_{D_o}}$ of $\beta = 0$ as shown above is only theoretically possible, it serves two purposes. First, all curves of $\frac{C_D}{C_{D_o}}$ vs AR $\tan\gamma$ for $0 < \beta < 1$ are essentially parallel to it, for very large AR $\tan\gamma$ Second, it can be considered as a standard to measure the wave drag for different wing planforms at different Mach numbers.

(d) In the range of $0 < \beta < 1$, the middle chord line (i.e. the maximum thickness line) along the span is supersonic. The wave drag in general is higher than the two-dimensional case, if AR $\tan\gamma$ is at the right of the line of cusps $\beta_o = 1$. $\frac{C_D}{C_{D_o}}$ curves are nearly parallel to $\frac{C_D}{C_{D_o}} = 1$ line ($\beta = 0$) when AR $\tan\gamma > 25$. Therefore, for the preliminary investigations, it is possible to extrapolate $\frac{C_D}{C_{D_o}}$ for AR $\tan\gamma$ beyond the given range. Also, $\frac{C_D}{C_{D_o}}$ increases with β for the same AR $\tan\gamma$. Theory shows $\frac{C_D}{C_{D_o}} \to \infty$ as AR $\tan\gamma \to \infty$. In this range $0 < \beta < 1$, $\frac{C_D}{C_{D_o}}$ is possible only at every small values of AR $\tan\gamma$.

(e) At $\beta = 1$, the right characteristic or Mach line coincides with the middle chord line on the right half span. For the taper ratio $\sigma = 0.2$, and the AR tan γ (> 7.6), the $\frac{C_D}{C_{D_o}}$ at $\beta = 1$ is the highest of all drag curves. But at AR tan γ $< \sqrt{2}$, the drag coefficient can be lower than that of the two-dimensional case.

For the taper ratio $\sigma = 0.5$, $\frac{C_D}{C_{D_o}}$ at $\beta = 1$ is not the highest of all $\frac{C_D}{C_{D_o}}$ at various values of β for a fixed AR tan γ .

(f) When $\beta > 1$, the middle chord line is subsonic. This family of drag curves changes slope twice, once at the line $\beta_1 = -1$ and again at the line $\beta_1 = 1$. In the region to the right of the line $\beta_1 = 1$, $\frac{C_D}{C_{D_o}}$ curves drop quickly at first, and then are asymptotic to the real axis as AR tan $\gamma \longrightarrow 1$. It has been shown in reference 2, based on the writer's investigation, that the total wave drag for an infinite wing with subsonic leading and trailing edges $\beta_o = \beta = \beta_1 > 1$ is finite although the wing area is infinite. Therefore, $C_D \longrightarrow 0$ as AR tan $\gamma \rightarrow \infty$ as long as $\beta > 1$. Besides, the larger the values of $\beta\,(> 1)$, the smaller the wave drag. In both graphs, $\frac{C_D}{C_{D_o}} < 1$ for $\beta > 1.1$. As $\beta \rightarrow 1$, the wave drag rises very quickly with larger values of AR tan γ .

As $\beta \longrightarrow \infty$, there are two possible cases: (i) $\gamma \longrightarrow 90^{\circ}$ if M > 1 but finite, and (ii) $M \longrightarrow 1$ if $|\gamma| < 90^{\circ}$. According to the equation, $\frac{C_D}{C_{D_o}} \longrightarrow 0$ as $\beta \longrightarrow \infty$. Case (i) is purely theoretical. Case (ii) gives $C_{D_o} \longrightarrow \infty$ as $M \longrightarrow 1$. Therefore, $\frac{C_D}{C_{D_o}} \longrightarrow 0$ as $M \longrightarrow 1$ does not necessarily mean $C_D = 0$. Actually, as $M \longrightarrow 1$ the linearized theory gives a finite value of wave drag as shown by the writer in reference 2.

According to these graphs, if $|\gamma| \neq 0$, $C_D \longrightarrow 0$ for all values of β as the aspect ratio goes to zero.

3.3 Special Cases of the Wave Drag Equation

Most of these special cases are required in calculating the curves shown in Figs. 2 and 3. Therefore, we have to write them down one by one. These special cases are based upon the taper ratio that is between 0 and 1.

(a) As $\beta_o \to 1$ expressions A and D in equation (3.21) take on the following limiting values while the rest of the equation stays the same except the expressions, $a = b = c = 0$.

$$A = \frac{(1-\nu'b'+b')^2}{2(\nu'-1)}\left[-\left(\frac{1-\nu'b'-b'}{1-\nu'b'+b'}\right)^{1/2}+\left(\frac{1-\nu'b'}{1-\nu'b'+b'}\right)^{1/2}\right]$$

$$+\frac{(1-\nu'b'+2b')^2}{2(\nu'-2)}\left[\left(\frac{1-\nu'b'-2b'}{1-\nu'b'+2b'}\right)^{1/2}-\left(\frac{1-\nu'b'}{1-\nu'b'+2b'}\right)^{1/2}\right]$$

$$D = \frac{1}{2\nu'}\left\{\sigma^{3/2}\left[(1-\nu'b'+b')^{1/2}-(1-\nu'b'+2b')^{1/2}\right]+\frac{2\nu'-1}{\nu'-1}(1-b')^{1/2}\right.$$

$$\left.-\frac{2(\nu'-1)}{(\nu'-2)}(1-2b')^{1/2}+\frac{\nu'}{(\nu'-1)(\nu'-2)}\right\} \qquad (3.22)$$

This case occurs when the right characteristic coincides with the leading edge on the right side.

(b) Similarly for $\beta_i = 1$ expressions B and E become

$$B = \frac{(1-\nu'b'-b')^2}{2(\nu'+1)}\left[\left(\frac{1-\nu'b'+b'}{1-\nu'b'-b'}\right)^{1/2}-\left(\frac{1-\nu'b'}{1-\nu'b'-b'}\right)^{1/2}\right]+\frac{(1-\nu'b'-2b')^2}{2(\nu'+2)}\left[-\left(\frac{1-\nu'b'+2b'}{1-\nu'b'-2b'}\right)^{1/2}+\left(\frac{1-\nu'b'}{1-\nu'b'-2b'}\right)^{1/2}\right]$$

$$E = \frac{1}{2\nu'}\left\{\sigma^{3/2}\left[-(1-\nu'b'-b')^{1/2}+(1-\nu'b'-2b')^{1/2}\right]-\frac{2\nu'+1}{\nu'+1}(1+b')^{1/2}\right.$$

$$\left.+\frac{2(\nu'+1)}{\nu'+2}(1+2b')^{1/2}+\frac{\nu'}{(\nu'+1)(\nu'+2)}\right\} \qquad (3.23)$$

The expression b = 0. All the other terms remain the same as shown in equation (3.21). This case occurs when the right characteristic coincides with the trailing edge on the right side.

(c) When $\beta = 1$, the expressions C and F are

$$C = \frac{(\sigma+2b')^2}{2(2-\nu')}\left[-\left(\frac{\sigma-2b'}{\sigma+2b'}\right)^{1/2}+\left(\frac{\sigma}{\sigma+2b'}\right)^{1/2}\right]+\frac{(\sigma-2b')^2}{2(2+\nu')}\left[-\left(\frac{\sigma+2b'}{\sigma-2b'}\right)^{1/2}+\left(\frac{\sigma}{\sigma-2b'}\right)^{1/2}\right]$$

$$F=\frac{1}{2\nu'}\left\{\sigma^{3/2}\left[-(\sigma+2b')^{1/2}+(\sigma-2b')^{1/2}\right]-\frac{2(1-\nu')}{2-\nu'}(1-2b')^{1/2}\right.$$

$$\left.+\frac{2(1+\nu')}{2+\nu'}(1+2b')^{1/2}-\frac{4\nu'}{(4-\nu'^2)}\right\} \qquad (3.24)$$

b = c = 0. All the rest remain the same as shown in equation (3.21). This occurs when the Mach line coincides with the maximum thickness line.

(d) When $\beta_0 = -1$, A and D become

A = B in equation (3.23) where $\beta_1 = 1$

D = E in equation (3.23) (3.25)

Here a = 0. The rest of the terms in equation (3.21) remain the same. This case occurs when the left characteristic coincides with the leading edge on the right side. This conforms with the reversed flow theorem, $\beta_0 = -1 \longrightarrow \beta_1 = 1$ if the flow direction is reversed.

When $\beta_1 = -1$, B and E become

$$B = A \text{ in equation (3.22) where } \beta_0 = 1$$
$$E = D \text{ in equation (3.22)} \qquad (3.26)$$

The terms $a = b = c = 0$. The rest of the terms remain the same as given in equation (3.21).

When $\beta = -1$, C and F are the same as given above for $\beta = 1$ with some rearrangement of terms. $a = c = 0$.

(e) When $\mathcal{D}' = 0$, or there is no taper $\beta_0 = \beta_1 = \beta$,

equation (3.21) becomes

$$\pi b' \frac{C_D}{C_{D_0}} = b'^2 \left\{ \frac{-3\beta}{(\beta^2-1)^{1/2}} \cosh^{-1}\left|\frac{\beta^2+1}{2\beta}\right| - \cosh^{-1}\left|\frac{1}{b'}\right| + 4\cosh^{-1}\left|\frac{1}{2b'}\right| \right\}$$

$$+ \left\{ \begin{array}{l} \dfrac{(1+\beta b')^2}{2\beta(1-\beta^2)^{1/2}} \left\{ -\sin^{-1}\dfrac{\beta+b'}{1+\beta b'} + \sin^{-1}\left[\beta + \dfrac{(1-\beta^2)b'}{2(1+\beta b')}\right] \right\} + \dfrac{(1+2\beta b')^2}{2\beta(1-\beta^2)^{1/2}} \left\{ \sin^{-1}\dfrac{\beta+2b'}{1+2\beta b'} - \sin^{-1}\left[\beta + \dfrac{(1-\beta^2)b'}{1+2\beta b'}\right] \right\} \\ \dfrac{(1+\beta b')^2}{2\beta(\beta^2-1)^{1/2}} \left\{ \cosh^{-1}\left|\dfrac{\beta+b'}{1+\beta b'}\right| - \cosh^{-1}\left|\beta + \dfrac{(1-\beta^2)b'}{2(1+\beta b')}\right| \right\} + \dfrac{(1+2\beta b')^2}{2\beta(\beta^2-1)^{1/2}} \left\{ -\cosh^{-1}\left|\dfrac{\beta+2b'}{1+2\beta b'}\right| + \cosh^{-1}\left|\beta + \dfrac{(1-\beta^2)b'}{1+2\beta b'}\right| \right\} \end{array} \right.$$

$$+ \left\{ \begin{array}{l} \dfrac{(1-\beta b')^2}{2\beta(1-\beta^2)^{1/2}} \left\{ -\sin^{-1}\dfrac{\beta-b'}{1-\beta b'} + \sin^{-1}\left[\beta - \dfrac{(1-\beta^2)b'}{2(1-\beta b')}\right] \right\} + \dfrac{(1-2\beta b')^2}{2\beta(1-\beta^2)^{1/2}} \left\{ \sin^{-1}\dfrac{\beta-2b'}{1-2\beta b'} - \sin^{-1}\left[\beta - \dfrac{(1-\beta^2)b'}{1-2\beta b'}\right] \right\} \\ \dfrac{(1-\beta b')^2}{2\beta(\beta^2-1)^{1/2}} \left\{ \cosh^{-1}\left|\dfrac{\beta-b'}{1-\beta b'}\right| - \cosh^{-1}\left|\beta - \dfrac{(1-\beta^2)b'}{2(1-\beta b')}\right| \right\} + \dfrac{(1-2\beta b')^2}{2\beta(\beta^2-1)^{1/2}} \left\{ \cosh^{-1}\left|\dfrac{\beta-2b'}{1-2\beta b'}\right| - \cosh^{-1}\left|\beta - \dfrac{(1-\beta^2)b'}{1-2\beta b'}\right| \right\} \end{array} \right.$$

$$+ \left\{ \begin{array}{l} \dfrac{1}{2\beta(1-\beta^2)^{1/2}} \left\{ \sin^{-1}\left[\beta + \dfrac{(1-\beta^2)b'}{2}\right] - \sin^{-1}\left[\beta + (1-\beta^2)b'\right] + \sin^{-1}\left[\beta - \dfrac{(1-\beta^2)b'}{2}\right] - \sin^{-1}\left[\beta - (1-\beta^2)b'\right] \right\} \\ \dfrac{1}{2\beta(\beta^2-1)^{1/2}} \left\{ -\cosh^{-1}\left|\beta + \dfrac{(1-\beta^2)b'}{2}\right| + \cosh^{-1}\left|\beta + (1-\beta^2)b'\right| - \cosh^{-1}\left|\beta - \dfrac{(1-\beta^2)b'}{2}\right| - \cosh^{-1}\left|\beta - (1-\beta^2)b'\right| \right\} \end{array} \right.$$

$$+ \left\{ \begin{array}{l} \dfrac{b'}{(1-\beta^2)^{1/2}} \left\{ \sin^{-1}\left[\beta - \dfrac{(1-\beta^2)b'}{2}\right] - \sin^{-1}\left[\beta + \dfrac{(1-\beta^2)b'}{2}\right] - 2\sin^{-1}\left[\beta + (1-\beta^2)\,b'\right] - 2\sin^{-1}\left[\beta - (1-\beta^2)\,b'\right] \right\} \\ \dfrac{b'}{(\beta^2-1)^{1/2}} \left\{ -\cosh^{-1}\left|\beta - \dfrac{(1-\beta^2)b'}{2}\right| + \cosh^{-1}\left|\beta + \dfrac{(1-\beta^2)b'}{2}\right| - 2\cosh^{-1}\left|\beta + (1-\beta^2)\,b'\right| + 2\cosh^{-1}\left|\beta - (1-\beta)\,b'\right| \right\} \end{array} \right.$$

$$+ \left\{ \begin{array}{l} \dfrac{1}{(1-\beta^2)^{1/2}} \left\{ \left(\dfrac{4}{(2+\beta b')^2 - b'^2}\right)^{1/2} - \left(\dfrac{4}{(2-\beta b')^2 - b'^2}\right)^{1/2} + \left(\dfrac{1}{(1+\beta b')^2 - b'^2}\right)^{1/2} + \left(\dfrac{1}{(1-\beta b')^2 - b'^2}\right)^{1/2} \right\} \\ \dfrac{1}{(\beta^2-1)^{1/2}} \left\{ \left(\dfrac{4}{(2+\beta b')^2 - b'^2}\right)^{1/2} + \left(\dfrac{4}{(2-\beta b')^2 - b'^2}\right)^{1/2} - \left(\dfrac{1}{(1+\beta b')^2 - b'^2}\right)^{1/2} - \left(\dfrac{1}{(1-\beta b')^2 - b'^2}\right)^{1/2} \right\} \end{array} \right.$$

(3.27)

The above equation is in accord with the results given in reference 2.

(f) If $M \to 1$, $\beta \to \pm\infty$ as γ is positive or negative.

Define

$$\mu = \frac{b}{a_0} \quad , \quad \nu' b' = \nu\mu \quad , \quad \omega = \mu \tan\gamma \, , \quad \omega_0 = \mu \tan\gamma_0 \, , \quad \omega_1 = \mu \tan\gamma_1$$

$$\frac{\pi C_D}{8\alpha^2}\left(\frac{2}{\sigma}-\nu\right) = 3\log\frac{1-\nu\mu}{\omega} + \frac{1}{2}\log\frac{\omega}{\omega_0} + \frac{1}{2}\log\frac{\omega}{\omega_1} - \log 2$$

$$+\frac{\omega}{\omega_0}\left(\frac{1}{\omega}+1\right)^2\left\{\log 2\left(\frac{1-\nu\mu}{1+\omega}\right) - \log\left(\frac{2+2\omega-\omega_0}{1+\omega}\right)\right\} + \frac{1}{2}\left(\frac{\omega}{\omega+\omega_0}\right)\left(\frac{1+\omega+\omega_0}{\omega_0}\right)^2\left\{-\log\frac{1-\nu\mu}{1+\omega+\omega_0} + \log\frac{1+\omega_0}{1+\omega+\omega_0}\right\}$$

$$+\frac{1}{2}\left(\frac{\omega}{\omega+\omega_1}\right)\left(\frac{1+\omega+\omega_1}{\omega}\right)^2\left\{-\log\frac{1-\nu\mu}{1+\omega+\omega_1} + \log\frac{1+\omega_1}{1+\omega+\omega_1}\right\} + \frac{1}{2}\frac{\omega_1}{\omega+\omega_1}\left(\frac{1-\omega-\omega_1}{\omega_1}\right)^2\left\{-\log\frac{1-\nu\mu}{1-\omega-\omega_1} + \log\frac{1-\omega_1}{1-\omega-\omega_1}\right\}$$

$$+\frac{1}{2}\left(\frac{\omega}{\omega+\omega_0}\right)\left(\frac{1-\omega-\omega_0}{\omega}\right)^2\left\{-\log\frac{1-\nu\mu}{1-\omega-\omega_0} + \log\frac{1-\omega_0}{1-\omega-\omega_0}\right\} + \frac{1}{2}\frac{\omega}{\omega_1}\left(\frac{1}{\omega}-1\right)^2\left\{\log\frac{1-\nu\mu}{1-\omega} - \log\left|1-\frac{\omega_1}{2(1-\omega)}\right|\right\}$$

$$+\frac{(1-\nu\mu)^2}{2\nu\mu\omega_0}\left\{\log\left[1+\frac{\omega_0}{2(1-\nu\mu)}\right] - \log\left(1+\frac{\omega_0}{1-\nu\mu}\right)\right\} + \frac{(1-\nu\mu)^2}{2\nu\mu\omega}\left\{-\log\left(1+\frac{\omega}{1-\nu\mu}\right) + \log\left(1-\frac{\omega}{1-\nu\mu}\right)\right\}$$

$$+\frac{(1-\nu\mu)^2}{2\nu\mu\omega_1}\left\{-\log\left[1-\frac{\omega_1}{2(1-\nu\mu)}\right] - \log\left(1-\frac{\omega_1}{1-\nu\mu}\right)\right\} + \frac{1}{2\nu\mu\omega_0}\left\{\left(1-\frac{\nu\mu}{\omega}\right)\log\left(\frac{2-\omega_0}{2}\right) - \left(\frac{\omega+\omega_0-2\nu\mu}{\omega+\omega_0}\right)\log(1-\omega_0)\right\}$$

$$+\frac{1}{2\nu\mu\omega}\left\{-\left(\frac{\omega+\omega_1-\nu\mu}{\omega+\omega_1}\right)\log(1-\omega) + \left(\frac{\omega+\omega_0+\nu\mu}{\omega+\omega_0}\right)\log(1+\omega) - \frac{4\nu\mu\omega}{(\omega+\omega_1)(\omega+\omega_0)}\right\}$$

$$+\frac{1}{2\nu\mu\omega_1}\left\{-\left(\frac{\omega+\nu\mu}{\omega}\right)\log\left(\frac{2+\omega_1}{2}\right) + \left(\frac{\omega+\omega_1+\nu\mu}{\omega+\omega_1}\right)\log(1+\omega_1) + \frac{\nu\mu\omega_1}{\omega(\omega+\omega_1)}\right\}$$

$$-\frac{1}{2}\left\{\frac{1}{\omega(\omega+\omega_0)}\right\} \qquad (3.28)$$

There are a number of other limiting cases such as $\beta_0 + \beta = 0$ $(\gamma_0 = -\gamma)$ and $\beta_1 + \beta = 0$ $(\gamma_1 = -\gamma)$ which are also required in calculation. If the taper ratio $\sigma = 0$ and $\beta_1 = 0$ equation (3.21) will give the wave

drag of the delta wing which checks with Puckett's results. Owing to limited space, they are all omitted.

IV. Aerodynamic Behavior of a Wing with a Given Lift Distribution

From equation (2.30)

$$g(\lambda,y) = \frac{1}{2\pi} \int_{-\infty}^{\infty} dt\ e^{-i\lambda t}\, C_p(t,y,+o) \tag{2.30}$$

Thus, when the pressure coefficient distribution $C_p(t,y,+o)$ is given on the wing planform, g (λ, y) can be obtained with this equation. Let us consider a tapered swept-back wing with a constant lift distribution

$$C_p(t,y) = C_{p_o} \qquad -b \le y \le b$$
$$\beta_o|y| - a_o' \le t \le \beta_1|y| + a_o'$$

where β_o, β_1 are defined in Figure 1. Thus at any y within the span, we have

$$g(\lambda,y) = \frac{1}{2\pi} \int_{\beta_o|y|-a_o'}^{\beta_1|y|+a_o'} C_{p_o}\, e^{-i\lambda t}\, dt$$

$$= \frac{i\,C_{p_o}}{2\pi\lambda} \left\{ e^{-i\lambda(\beta_1|y|+a_o')} - e^{-i\lambda(\beta_o|y|-a_o')} \right\} \tag{4.1}$$

As $\lambda \longrightarrow 0$ we can evaluate g (0, y) as

$$g(0,y) = \frac{C_{p_0}}{\pi}\left\{ a_0' - \frac{\beta_0-\beta_1}{2}|y| \right\} \tag{4.2}$$

Substituting the above equation in equation (2.42), we have

$$w(t,y,+0) = \frac{-m'U}{2}\int_{-b}^{b}\frac{d\eta}{(y-\eta)^2}\left\{\frac{C_{p_0}}{\pi}\left(a_0' - \frac{\beta_0-\beta_1}{2}|\eta|\right)\right.$$
$$\left. + \frac{|y-\eta|}{2}\int_{-\infty}^{\infty} d\lambda \frac{C_{p_0}}{2\pi\lambda i}\left(e^{-i\lambda(\beta_1|y|+a_0')} - e^{-i\lambda(\beta_0|y|-a_0')}\right)e^{i\lambda t}H_1^{(2)}(\lambda|y-\eta|)\right\}$$

$$= \frac{-m'UC_{p_0}}{2\pi}\int_{-b}^{b}\frac{d\eta}{(y-\eta)^2}\left\{\left(a_0' - \frac{\beta_0-\beta_1}{2}|\eta|\right)\right.$$
$$\left. - \frac{i}{2}\cdot\frac{|y-\eta|}{2}\int_{-\infty}^{\infty}\frac{d\lambda}{\lambda}\left[e^{-i\lambda(\beta_1|y|+a_0')} - e^{-i\lambda(\beta_0|y|-a_0')}\right]e^{i\lambda t}H_1^{(2)}(\lambda|y-\eta|)\right\} \tag{4.3}$$

With the aid of Appendix B, we can evaluate the infinite integrals and can show

$$w(t,y,+o) = \frac{-C_{p_o} m' U}{2\pi} \int_{-b}^{b} \frac{d\eta}{(y-\eta)^2} \left[\left(a_o' - \frac{\beta_o - \beta_1}{2}|\eta|\right) \right.$$

$$- \frac{|y-\eta|}{2} \begin{cases} -\dfrac{t_1 - \beta_1|\eta|}{|y-\eta|} & (t_1 - \beta_1|\eta| \le |y-\eta|) \\ -\dfrac{t_1 - \beta_1|\eta|}{|y-\eta|} + 2\dfrac{\sqrt{(t_1-\beta_1|\eta|)^2 - (y-\eta)^2}}{|y-\eta|} & (t_1 - \beta_1|\eta|) \ge |y-\eta|) \end{cases}$$

$$\left. - \frac{|y-\eta|}{2} \begin{cases} \dfrac{t_o - \beta_o|\eta|}{|y-\eta|} & (t_o - \beta_o|\eta| \le |y-\eta|) \\ \dfrac{t_o - \beta_o|\eta|}{|y-\eta|} - 2\dfrac{\sqrt{(t_o-\beta_o|\eta|)^2 - (y-\eta)^2}}{|y-\eta|} & (t_o - \beta_o|\eta|) \ge |y-\eta|) \end{cases} \right] \qquad (4.4)$$

where $t_o = t + a_o'$, $t_1 = t - a_o'$. Only one of the two expressions holds for the range specified in the bracket.

If we write the integration of η from 0 to b only, we have

$$w(t,y,+0) = \frac{-C_{p_0} m' U}{4\pi} \int_0^b d\eta \left\{ \frac{2a_0' - (\beta_0 - \beta_1)\eta}{(y-\eta)^2} + \frac{2a_0' - (\beta_0 - \beta_1)\eta}{(y+\eta)^2} - \frac{2a_0' - (\beta_0 - \beta_1)\eta}{(y-\eta)^2} \right.$$

$$+ \frac{2a_0' - (\beta_0 - \beta_1)\eta}{(y+\eta)^2} - \frac{2\sqrt{(t_0 - \beta_0\eta)^2 - (y-\eta)^2}}{(y-\eta)^2} - \frac{2\sqrt{(t_0 - \beta_0\eta)^2 - (y+\eta)^2}}{(y+\eta)^2}$$

$$\left. + \frac{2\sqrt{(t_1 - \beta_1\eta)^2 - (y-\eta)^2}}{(y-\eta)^2} + \frac{2\sqrt{(t_1 - \beta_1\eta)^2 - (y+\eta)^2}}{(y+\eta)^2} \right\}$$

$$= \frac{-C_{p_0} m' U}{2\pi} \int_0^b d\eta \left\{ \frac{\sqrt{(t_0 - \beta_0\eta)^2 - (y-\eta)^2}}{(y-\eta)^2} - \frac{\sqrt{(t_1 - \beta_1\eta)^2 - (y-\eta)^2}}{(y-\eta)^2} \right.$$

$$\left. + \frac{\sqrt{(t_0 - \beta_0\eta)^2 - (y+\eta)^2}}{(y+\eta)^2} - \frac{\sqrt{(t_1 - \beta_1\eta)^2 - (y+\eta)^2}}{(y+\eta)^2} \right\}$$

(4.5)

where $t_0 - t_1 = 2a_0'$ is used so that the first terms cancel out.

Now carrying out the integration with respect to η

$$w(t,y,+0) = \frac{C_{p_0} m' U}{2\pi} \left\{ -(A-B) + (C-D) \right\}$$

(4.6)

where

$$A = \int_0^b d\eta \, \frac{\sqrt{(t_0-\beta_0\eta)^2-(y-\eta)^2}}{(y-\eta)^2} \qquad \text{(See Table A)} \tag{4.7}$$

$$B = \int_0^b d\eta \, \frac{\sqrt{(t_1-\beta_1\eta)^2-(y-\eta)^2}}{(y-\eta)^2} \qquad \text{(See Table B)} \tag{4.8}$$

$$C = -\int_0^b d\eta \, \frac{\sqrt{(t_0-\beta_0\eta)^2-(y+\eta)^2}}{(y+\eta)^2} \qquad \text{(See Table C)} \tag{4.9}$$

$$D = -\int_0^b d\eta \, \frac{\sqrt{(t_1-\beta_1\eta)^2-(y+\eta)^2}}{(y+\eta)^2} \qquad \text{(See Table D)} \tag{4.10}$$

The present treatment is equivalent to considering two hypothetical wings. The first one is of constant positive lift distribution (C_{p_o} is an assigned constant) starting at the leading edge extending downstream to infinity with semi-span = b. The second wing is of constant negative lift distribution (C_{p_o} is assigned negative constant) starting at the trailing edge and also extending downstream to infinity with semi-span b. The superposition of both hypothetical wings gives the aerodynamical behavior of the actual wing.

Integral A, equation (4.7), gives the contribution of downwash due to right-side area of the first hypothetical wing in the forward Mach cone of the point P (t, y). Similarly, Integral C, equation (4.9), gives the contribution for the area on the left side.

On the other hand, integral B, equation (4.8), gives the contribution of the right side of the second hypothetical wing. Similarly integral D, equation (4.10), gives the left side contribution.

As far as the limits of integrals are concerned, each holds for within the limit 0 to b, whenever the integrand is a positive real quantity. However, for many locations of P (t, y), the integrand is positive only in a much narrower range of η than the interval (0, b). In order to determine the valid range of the integrals and their respective values for all possible locations of P, Tables A, B, C, and D are tabulated. The corresponding values of the integrals

for the different cases are given in the right-hand columns of the Tables.

Take Table A as an example. If the leading edge is subsonic ($\beta_o > 1$), the lower limit of η is always zero because the forward Mach cone at P always intersects the wing center line within the wing area. When $\beta_o > 1$ the upper limit of η is given in the upper half of Table A. Condition 1 concerns the location of the point P, which may be ahead, on or behind the leading edge, while condition 2 concerns the right intersection of the forward Mach cone of P with the leading edge, or side edge. Under both conditions 1 and 2, we have 6 possible cases. The upper limit of η is given in each case, and the value of the integral A is also given accordingly.

If the leading edge is supersonic ($\beta_o < 1$), the integral A exists only when the point P is behind the leading edge. In particular, both the upper and the lower limit may vary within the interval (0-b). The condition for the lower limit depends on the intersection of the left side of the forward Mach cone of P. It is zero when and only when the intersection is on the center line of the wing in the wing area. If the intersection is on the right side leading edge, the lower limit is $\frac{y - t_o}{1 - \beta_o}$ as indicated. The condition on the upper limit depends on the right hand intersection of the forward Mach cone of P. If the right side of forward Mach cone cuts the leading edge within the span, the upper limit is $\frac{t_o + y}{1 + \beta_o}$; otherwise, the upper limit of η is b.

The other 3 tables can be explained similarly. Figure 6 shows 4 typical cases concerning the integral limits. Figure 6 (a) shows the forward Mach cone of a point P (t, y) that lies only in the right side area of the wing. Therefore only integral A exists and all the other three integrals are zero. Since the leading edge is supersonic ($\beta_o < 1$), the upper integral limit is $\frac{t_o + y}{1 + \beta_o}$. It belongs to A-9 as indicated, according to Table A. Figure 6 (b) shows the forward Mach cone covering both the left and right side area of the wing. Thus, only integrals A and C exist. The integrals are indicated. Figure 6(c) and 6(d) can be similarly explained.

TABLE A

Integration Limits of η and the Corresponding Values of the Integral A

	$\beta_0 > 1$ (The lower limit is always zero.)			
	Condition 1	Condition 2	Upper limit	A
1	$t_0 > \beta_0 y$	$\frac{t_0 - y}{\beta_0 - 1} < b$	$\frac{t_0 - y}{\beta_0 - 1}$	$\frac{\sqrt{t_0^2 - y^2}}{y} + \beta_0 \cosh^{-1}\frac{t_0}{y} + \sqrt{\beta_0^2 - 1}\,\cosh^{-1}\frac{y - \beta_0 t_0}{t_0 - \beta_0 y}$
2	$t_0 > \beta_0 y$	$\frac{t_0 - y}{\beta_0 - 1} \geq b$	b	$\frac{\sqrt{t_0^2 - y^2}}{y} + \beta_0 \cosh^{-1}\frac{t_0}{y} + \sqrt{\beta_0^2 - 1}\,\cosh^{-1}\frac{y - \beta_0 t_0}{t_0 - \beta_0 y}$ $- \frac{\sqrt{(t_0 - \beta_0 b)^2 - (y - b)^2}}{y - b} - \beta_0 \cosh^{-1}\frac{t_0 - \beta_0 b}{y - b} - \sqrt{\beta_0^2 - 1}\,\cosh^{-1}\frac{(\beta_0^2 - 1)b + y - \beta_0 t_0}{t_0 - \beta_0 y}$
3	$t_0 = \beta_0 y$	$y < b$	y	∞
4	$t_0 = \beta_0 y$	$y \geq b$	b	∞
5	$t_0 < \beta_0 y$	$\frac{t_0 + y}{\beta_0 + 1} < b$	$\frac{t_0 + y}{\beta_0 + 1}$	$\frac{\sqrt{t_0^2 - y^2}}{y} + \beta_0 \cosh^{-1}\frac{t_0}{y} + \sqrt{\beta_0^2 - 1}\,\cosh^{-1}\frac{y - \beta_0 t_0}{t_0 - \beta_0 y}$
6	$t_0 < \beta_0 y$	$\frac{t_0 + y}{\beta_0 + 1} \geq b$	b	$- \frac{\sqrt{(t_0 - \beta_0 b)^2 - (y - b)^2}}{y - b} - \beta_0 \cosh^{-1}\frac{t_0 - \beta_0 b}{y - b} - \sqrt{\beta_0^2 - 1}\,\cosh^{-1}\frac{(\beta_0^2 - 1)b + y - \beta_0 t_0}{t_0 - \beta_0 y}$ $\frac{\sqrt{t_0^2 - y^2}}{y} + \beta_0 \cosh^{-1}\frac{t_0}{y} + \sqrt{\beta_0^2 - 1}\,\cosh^{-1}\frac{y - \beta_0 t_0}{t_0 - \beta_0 y}$

TABLE A CONTINUED

$\beta_o < 1$ (The integral exists only when $t_o > \beta_o y$.)					
	Condition	Lower Limit	Condition	Upper Limit	A
7	$\frac{y-t_o}{1-\beta_o} \leq 0$	0	$\frac{t_o+y}{1+\beta_o} < b$	$\frac{t_o+y}{1+\beta_o}$	$\frac{\pi}{2}\sqrt{1-\beta_o^2} + \frac{\sqrt{t_o^2-y^2}}{y} + \beta_o \cosh^{-1}\frac{t_o}{y} + \sqrt{1-\beta_o^2}\sin^{-1}\frac{y-\beta_o t_o}{t_o-\beta_o y}$
8	$\frac{y-t_o}{1-\beta_o} \leq 0$	0	$\frac{t_o+y}{1+\beta_o} \geq b$	b	$\frac{\sqrt{t_o^2-y^2}}{y} + \beta_o \cosh^{-1}\frac{t_o}{y} + \sqrt{1-\beta_o^2}\sin^{-1}\frac{y-\beta_o t_o}{t_o-\beta_o y} - \frac{\sqrt{(t_o-\beta_o b)^2-(y-b)^2}}{y-b}$ $-\beta_o \cosh^{-1}\frac{t_o-\beta_o b}{y-b} - \sqrt{1-\beta_o^2}\sin^{-1}\frac{-b(1-\beta_o^2)+y-\beta_o t_o}{t_o-\beta_o y}$
9	$\frac{y-t_o}{1-\beta_o} > 0$	$\frac{y-t_o}{1-\beta_o}$	$\frac{t_o+y}{1+\beta_o} < b$	$\frac{t_o+y}{1+\beta_o}$	$\pi\sqrt{1-\beta_o^2}$
10	$\frac{y-t_o}{1-\beta_o} > 0$	$\frac{y-t_o}{1-\beta_o}$	$\frac{t_o+y}{1+\beta_o} \geq b$	b	$\frac{\pi}{2}\sqrt{1-\beta_o^2} - \frac{\sqrt{(t_o-\beta_o b)^2-(y-b)^2}}{y-b} - \beta_o \cosh^{-1}\frac{t_o-\beta_o b}{y-b}$ $-\sqrt{1-\beta_o^2}\sin^{-1}\frac{-b(1-\beta_o^2)+y-\beta_o t_o}{t_o-\beta_o y}$

Table B may be obtained from Table A by merely substituting β, for β_o, and t, for t_o.

TABLE C

Integration Limits of η and the Corresponding Values of the Integral C

	$\beta_o > 1$		
	Condition	Upper Limit	C
1	$\frac{t_o - y}{1+\beta_o} < b$	$\frac{t_o - y}{1+\beta_o}$	$\frac{\sqrt{t_o^2 - y^2}}{y} + \beta_o \cosh^{-1}\frac{t_o}{y} - \sqrt{\beta_o^2 - 1}\,\cosh^{-1}\frac{-(y+\beta_o t_o)}{t_o + \beta_o y}$
2	$\frac{t_o - y}{1+\beta_o} \geq b$	b	$\frac{\sqrt{t_o^2 - y^2}}{y} + \beta_o \cosh^{-1}\frac{t_o}{y} - \sqrt{\beta_o^2 - 1}\,\cosh^{-1}\frac{-(y+\beta_o t_o)}{t_o + \beta_o y}$ $- \frac{\sqrt{(t_o^2 - \beta_o b)^2 - (y+b)^2}}{y+b} - \beta_o \cosh^{-1}\frac{t_o - \beta_o b}{y+b}$ $- \sqrt{\beta_o^2 - 1}\,\cosh^{-1}\frac{(\beta_o^2 - 1)b - (y+\beta_o t_o)}{t_o + \beta_o y}$
	$\beta_o < 1$		
	Condition	Upper Limit	C
3	$\frac{t_o - y}{1+\beta_o} < b$	$\frac{t_o - y}{1+\beta_o}$	$\frac{\pi}{2}\sqrt{1-\beta_o^2} + \frac{\sqrt{t_o^2 - y^2}}{y} + \beta_o \cosh^{-1}\frac{t_o}{y} - \sqrt{1-\beta_o^2}\sin^{-1}\frac{y+\beta_o t_o}{t_o + \beta_o y}$
4	$\frac{t_o - y}{1+\beta_o} \geq b$	b	$\frac{\sqrt{t_o^2 - y^2}}{y} + \beta_o \cosh^{-1}\frac{t_o}{y} - \sqrt{1-\beta_o^2}\sin^{-1}\frac{y+\beta_o t_o}{t_o + \beta_o y}$ $- \frac{\sqrt{(t_o^2 - \beta_o b)^2 - (y+b)^2}}{y+b} - \beta_o \cosh^{-1}\frac{t_o - \beta_o b}{y+b}$ $+ \sqrt{1-\beta_o^2}\sin^{-1}\frac{b(1-\beta_o^2) + (y+\beta_o t_o)}{t_o + \beta_o y}$

The integral C exists only when $t_o > y$. The lower limit is always zero.

Table D may be obtained from Table C by substituting β_1 for β_o, and t_1 for t_o.

Although the lift distribution of the wing with supersonic trailing edge is well known, the downwash may be interesting to explore. Figure 7 shows three infinite half wings with trailing edge at 15°, 30°, and 45° from the leading edge which is normal to the direction of flight. This is shown in the (t, y) plane, or the (x, y) plane with Mach number = $\sqrt{2}$. A negative infinite downwash always occurs at the tip. The curves are plotted as $\frac{2\pi w(y/t)}{m' C_{p_o} U}$ As we know $C_{p_o} = \frac{2\alpha_1}{m'}$ where α_1 = angle of attack of the wing, we can write $\frac{\pi w}{\alpha_1 U}$ vs $\frac{y}{t}$. Between the tip cone and the wing, the downwash is constant but increases with increasing trailing edge angle. Owing to the conical flow, the downwash is identically the same along the radial lines expressed in the conical coordinate $\frac{y}{t}$. The above curves were calculated with equation (4.6) and Tables A and B by setting $\beta_o = 0$, β_1 = tan 15°, tan 30°, tan 45° respectively and $a_o' = 0$. (Here $t = t_o = t_1$).

Figure 8 shows a wing tip of unit chord with raked angle = 30°. At $t = 0.5$, it behaves exactly the same as the 30° case of Figure 7, but at $t = 1.5$, it is quite different. Two infinite downwashes occur, one at the center of the leading edge tip cone, and the other at the center of the trailing edge tip cone. The former remains negative, the latter positive. Outside the two tip Mach cones, the downwash is identically zero as predicted by the two-dimensional theory. The above can be calculated from equation (4.6) and Tables A, B, and C by letting $\beta_o = \beta_1 = \tan 30°$, $a_o' = .5$ (Here $t = t_o - .5 = t_1 + .5$)

As another interesting example, the downwash distribution near the nose of an infinite constant chord swept-back wing is calculated (Fig. 9). The leading edge is swept-back at 30° but is still supersonic. The downwash at different locations on the span are plotted along t. In this case, the curves are plotted with $\frac{\sqrt{1-\beta_o^2}}{\alpha_1} \times \frac{w(t,y)}{U}$ vs. t at different values of y where $C_{p_o} = \frac{2\alpha_1}{m'\sqrt{1-\beta_o^2}}$ is introduced.

At $y = 0$, the downwash angle reaches the maximum value (0.8165) at a single nose point and remains zero along the chord up to the trailing edge. There the downwash angle is negative and equal to the maximum value in magnitude and recovers to zero downwash downstream. For instance at $y = 0.4$, the downwash angle is constant in the supersonic region, and drops down under the influence of the nose Mach cone. At the trailing edge, the downwash angle drops to a negative value abruptly and continues to decrease until the trailing mach cone is reached. The drop of downwash at the trailing edge is exactly equal to the downwash angle at the supersonic leading edge. Further along t, the downwash angle rises up again and becomes asymptotic to 0 as $t \longrightarrow \infty$. The same can be applied at any y until the nose Mach cone is off the trailing edge.

As another example, the downwash of a finite delta wing with 60° swept-back angle is calculated. Figure 10 shows the downwash distributions at different y. Figure 11 shows the downwash distribution of a tapered swept-back wing. The taper ratio is $\sigma = 1/6$. Figure 12 shows the downwash of the same swept-back wing far downstream. It is very interesting to examine the effect of different Mach cones on the downwash. One important feature of the subsonic leading edge is the infinite downwash angle. As before, the above are calculated with equation (4.6) and Tables A, B, C, and D.

The present approach on calculating downwash of a wing with constant lift distribution cannot be applied to wings with subsonic trailing edge, because the Joukowsky-Kutta condition must be satisfied at such trailing edge. In order to investigate the case with subsonic trailing edge, it is necessary to assume the distribution of the pressure coefficient drops to zero at the trailing edge.

Similarly, with the given pressure distribution, it is easy to calculate the side wash; the details are omitted.

The above gives just a case with simple pressure distribution along the chord to demonstrate the application of the method. Of course, the method is not limited to this case alone. At present, some investigation is under way for the roof-type pressure distribution along the chord.

References

1. von Kármán, Th., Neu Darstellung der Tragflügeltheorie, Zeitschrift f. angew. Math. u. Mech. (1935) 15, pp. 56-61.
2. von Kármán, Th., Supersonic Aerodynamics - Principle and Application, Jour. Aero. Sci. (July 1949) Vol. 17, No. 7, pp. 373-409.
3. Busemann, A., Infinitesimale Kegelige Ueberschallstroemung Sonderdruck, Jahrbuch 1942-43 der Deutschen Akademie der Luftfahrtforschung, (1943) Vol. 7B, No. 3, pp. 105-122. Also NACA TM No. 1100.
4. Lagerstrom, P. A., Linearized Supersonic Theory of Conical Wings. NACA TN No. 1685, (August 1948).
5. Hayes, W. D., Linearized Supersonic Flow, California Institute of Technology, Pasadena, (Thesis) (1947).
6. Stewart, H. J., The Lift of a Delta Wing at Supersonic Speeds, Quart. Appl. Math. (1946) Vol. 4 No. 3, pp. 246-254.
7. Laporte, O. and Bartels, R. C. F., An investigation of the Exact Solutions of the Linearized Equations for the Flow Past Conical Bodies, Bumblebee Series Rept. No. 75,(February 1948).
8. Snow, R. M., Aerodynamics of Thin Quadrilateral Wings at Supersonic Speeds, Quart. Appl. Math. (January 1948), Vol. 5, No. 4, pp. 417-428.
9. Jones, R. T., Properties of Low-Aspect-Ratio Pointed Wings at Speeds below and above the Speed of Sound, NACA TN No. 1032 (1946).

References

10. Jones, R. T., The Oblique Airfoils at Supersonic Speed, NACA TN No. 1107 (Sept. 1946).

11. Puckett, A. E., Supersonic Wave Drag of Thin Airfoils, Jour. Aero. Sci. (Sept. 1946) Vol. 13, No. 9, pp. 475-484.

12. Evaard, J. C., The Distribution of Wave Drag and Lift in the Vicinity of Wing Tips at Supersonic Speeds, NACA TN No. 1382, (July 1947).

13. Evaard, J. C., Theoretical Distribution of Lift on Thin Wings at Supersonic Speeds (An extension), NACA TN No. 1585 (1948).

14. Heaslet, M. A., Lomax, H., and Jones, A. L., Volterra's Solution of the Wave Equation as Applied to Three-dimensional Supersonic Airfoil Problems, NACA TN No. 1412, (1947).

15. Heaslet, M. A., and Lomax, H., The Use of Source Sink and Doublet Distributions Extended to the Solution of Arbitrary Boundary Value Problems in Supersonic Flow, NACA TN No. 1515 (1948).

16. Gunn, J. C., Linearized Supersonic Airfoil Theory, Part I and II, Phil. Trans. Roy. Soc. London (Dec. 1947), Series A Vol. 240 No. 820, pp. 327-373.

17. Lamb, H., Hydrodynamics, Cambridge Press, (1932).

18. Titchmarch, E. C., Fourier Integral, Oxford, (1937).

19. Watson, G. N., Theory of Bessel Functions, MacMillan, (1944).

20. von Kármán, Th., Some Investigations on Transonic and Supersonic Flow, Sixth International Congress for Applied Mechanics, (1948) (to be published).

References

21. Brown, C. E., Theoretical Lift and Drag of Thin Triangular Wings at Supersonic Speeds, NACA TN No. 1183 (1947).

Appendix A

Fourier Transform of the Slope Distribution on an Airfoil

As an example, the Fourier transform of the slope on a double-wedge airfoil is calculated. Fig. A-1 shows the shape and slope of a double wedge airfoil on a swept-back wing at a distance y from the center of the wing span. The slope distribution is as follows:

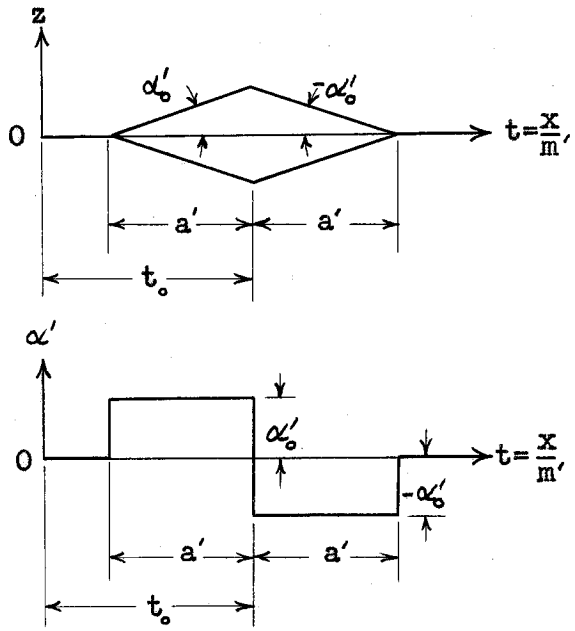

Fig. A-1

$$\alpha(t,y) = 0 \qquad t < t_o(y) - a'(y)$$

$$= \alpha_o'(y) \qquad t_o(y) - a'(y) < t \leq t_o$$

$$= -\alpha_o'(y) \qquad t_o \leq t < t_o(y) + a'(y)$$

$$= 0 \qquad t > t_o(y) + a'(y)$$

(A-1)

where α, α_o', t_o and a' are functions of y in general. Substituting the equation (A-1) into the equation (2.19) it yields

$$f(\lambda,y) = f_o(\lambda,y) + i f_1(\lambda,y)$$

$$= \frac{1}{2\pi}\int_{-\infty}^{\infty} \alpha(t,y)\, e^{-i\lambda t}\, dt$$

$$= \frac{\alpha_o'}{2\pi}\int_{t_o-a'}^{t_o} e^{-i\lambda t}\, dt \; - \frac{\alpha_o'}{2\pi}\int_{t_o}^{t_o+a'} e^{-i\lambda t}\, dt$$

$$= \frac{\alpha_o'}{2\pi}\, e^{-i\lambda t_o}\left\{ \int_{-a'}^{o} e^{-i\lambda\tau}\, d\tau - \int_{o}^{a'} e^{-i\lambda\tau}\, d\tau \right\} \qquad \text{(A-2)}$$

where $t = t_o + \tau$ is used in substitution. It is easy to show that

$$f(\lambda,y) = \frac{-\alpha_o'}{i\pi\lambda}\, e^{-i\lambda t_o}(1-\cos\lambda a') \qquad \text{(A-3)}$$

$$f_o(\lambda,y) = \frac{\alpha_o'}{\pi\lambda}\sin\lambda t_o\,(1-\cos\lambda a') \qquad \text{(even with respect to } \lambda\text{)} \qquad \text{(A-4)}$$

$$f_1(\lambda,y) = \frac{\alpha_o'}{\pi\lambda}\cos\lambda t_o\,(1-\cos\lambda a') \qquad \text{(Odd with respect to } \lambda\text{)} \qquad \text{(A-5)}$$

For a rectangular wing with constant airfoil section, where α_o', t_o and a' are independent of y in the span, equations (A-4) and (A-5) reduce to

$$f_o(\lambda, y) = 0$$

$$f_1(\lambda, y) = \frac{\alpha_o'}{\pi\lambda}(1-\cos\lambda a')$$

if we choose $t_o = 0$.

For the case of straight tapered swept-back wing, as shown in Fig. 1, we have

$$a'(y) = \frac{a_o - \nu|y|}{m'}$$

$$t_o(y) = \beta|y|$$

$$\alpha_o'(y) = \alpha_o' \quad \text{independent of y.}$$

For the details of the definitions of the different parameters refer to the figure. We have

$$f_o(\lambda, y) = \frac{\alpha_o'}{\pi\lambda}\sin(\lambda\beta|y|)(1-\cos\lambda a_y')$$

$$f_1(\lambda, y) = \frac{\alpha_o'}{\pi\lambda}\cos(\lambda\beta|y|)(1-\cos\lambda a_y')$$

(A-6)

Now, we can write

$$f(\lambda,y)\overline{f(\lambda,\eta)} = \left\{\frac{-\alpha_o'}{i\pi\lambda}\, e^{-i\lambda\beta|y|}(1-\cos\lambda a_y')\right\}\left\{\frac{\alpha_o'}{i\pi\lambda}\, e^{i\lambda\beta|\eta|}(1-\cos\lambda a_\eta')\right\}$$

$$= \frac{\alpha_o'^2}{\pi^2\lambda^2}\, e^{-i\lambda\beta(|y|-|\eta|)}(1-\cos\lambda a_y')(1-\cos\lambda a_\eta')$$

$$= \frac{\alpha_o'^2}{\pi^2\lambda^2}(1-\cos\lambda a_y')(1-\cos\lambda a_\eta')\left\{\cos\lambda\beta(|y|-|\eta|) - i\sin\lambda\beta(|y|-|\eta|)\right\}$$

$$= \left\{f_o(\lambda,y)f_o(\lambda,\eta) + f_1(\lambda,y)f_1(\lambda,\eta)\right\} + i\left\{f_1(\lambda,y)f_o(\lambda,\eta) - f_o(\lambda,y)f_1(\lambda,\eta)\right\}$$

(A-7)

Therefore separating the real and imaginary parts, we have

$$f_o(\lambda,y)f_o(\lambda,\eta) + f_1(\lambda,y)f_1(\lambda,\eta)$$

$$= \frac{\alpha_o'^2}{\pi^2\lambda^2}(1-\cos\lambda a_y')(1-\cos\lambda a_\eta')\cos\lambda\beta(|y|-|\eta|)$$

(A-8)

$$-f_1(\lambda,y)f_o(\lambda,\eta) + f_o(\lambda,y)f_1(\lambda,\eta)$$

$$= \frac{\alpha_o'^2}{\pi^2\lambda^2}(1-\cos\lambda a_y')(1-\cos\lambda a_\eta')\sin\lambda\beta(|y|-|\eta|)$$

(A-9)

Appendix B

The following are the integrals which are used so often in the text and many of which are not available in the ordinary handbook.

$$\int du \sin^{-1}\left(\frac{K}{u} \mp \beta\right) = u \sin^{-1}\left(\frac{K}{u} \mp \beta\right) + \begin{cases} \dfrac{\pm K}{(1-\beta^2)^{1/2}} \cosh^{-1}\left\{\beta \pm (1-\beta^2)\dfrac{u}{K}\right\} \\ \dfrac{\mp K}{(\beta^2-1)^{1/2}} \sin^{-1}\left\{\beta \mp (\beta^2-1)\dfrac{u}{K}\right\} \end{cases} *$$

$$\int du \sin^{-1}\left(\beta \mp \frac{K}{u}\right) = \sin^{-1}\left(\beta \mp \frac{K}{u}\right) + \begin{cases} \dfrac{\mp K}{(1-\beta^2)^{1/2}} \cosh^{-1}\left\{(1-\beta^2)\dfrac{u}{K} \pm \beta\right\} \\ \dfrac{\mp K}{(\beta^2-1)^{1/2}} \sin^{-1}\left\{(\beta^2-1)\dfrac{u}{K} \mp \beta\right\} \end{cases}$$

$$\int du \cosh^{-1}\left(\frac{K}{u} \mp \beta\right) = u \cosh^{-1}\left(\frac{K}{u} \mp \beta\right) + \begin{cases} \dfrac{\pm K}{(1-\beta^2)^{1/2}} \sin^{-1}\left\{\beta \pm (1-\beta^2)\dfrac{u}{K}\right\} \\ \dfrac{\mp K}{(\beta^2-1)^{1/2}} \cosh^{-1}\left\{\beta \mp (\beta^2-1)\dfrac{u}{K}\right\} \end{cases}$$

$$\int du \cosh^{-1}\left(\beta \mp \frac{K}{u}\right) = u \cosh^{-1}\left(\beta \mp \frac{K}{u}\right) + \begin{cases} \dfrac{\mp K}{(1-\beta^2)^{1/2}} \sin^{-1}\left\{(1-\beta^2)\dfrac{u}{K} \pm \beta\right\} \\ \dfrac{\mp K}{(\beta^2-1)^{1/2}} \cosh^{-1}\left\{(\beta^2-1)\dfrac{u}{K} \mp \beta\right\} \end{cases}$$

$$\int u\,du \sin^{-1}\left(\frac{K}{u} \mp \beta\right) = \frac{u^2}{2} \sin^{-1}\left(\frac{K}{u} \mp \beta\right) + \begin{cases} \dfrac{K^2}{2(1-\beta^2)^{3/2}}\left\{-\beta \cosh^{-1}\left[\beta \pm (1-\beta^2)\dfrac{u}{K}\right] + \sqrt{\left[\beta + (1-\beta^2)\dfrac{u}{K}\right]^2 - 1}\right\} \\ \dfrac{K^2}{2(\beta^2-1)^{3/2}}\left\{-\beta \sin^{-1}\left[\beta \mp (\beta^2-1)\dfrac{u}{K}\right] - \sqrt{1-\left[\beta \mp (\beta^2-1)\dfrac{u}{K}\right]^2}\right\} \end{cases}$$

$$\int u\,du \sin^{-1}\left(\beta \mp \frac{K}{u}\right) = \frac{u^2}{2} \sin^{-1}\left(\beta \mp \frac{K}{u}\right) + \begin{cases} \dfrac{K^2}{2(1-\beta^2)^{3/2}}\left\{\beta \cosh^{-1}\left[(1-\beta^2)\dfrac{u}{K} \pm \beta\right] \mp \sqrt{\left[(1-\beta^2)\dfrac{u}{K} \pm \beta\right]^2 - 1}\right\} \\ \dfrac{K^2}{2(\beta^2-1)^{3/2}}\left\{-\beta \sin^{-1}\left[(\beta^2-1)\dfrac{u}{K} \mp \beta\right] \pm \sqrt{1-\left[(\beta^2-1)\dfrac{u}{K} - \beta\right]^2}\right\} \end{cases}$$

*In all these formulas, the upper line corresponds to $\beta < 1$, and the lower line to $\beta > 1$.

$$\int u\,du\cosh^{-1}\left(\frac{K}{u}\mp\beta\right)=\frac{u^2}{2}\cosh^{-1}\left(\frac{K}{u}\mp\beta\right)+\begin{cases}\dfrac{K^2}{2(1-\beta^2)^{3/2}}\left\{-\beta\sin^{-1}\left[\beta\pm(1-\beta^2)\dfrac{u}{K}\right]-\sqrt{1-\left[\beta\pm(1-\beta^2)\dfrac{u}{K}\right]^2}\right\}\\[2ex]\dfrac{K^2}{2(\beta^2-1)^{3/2}}\left\{-\beta\cosh^{-1}\left[\beta\mp(\beta^2-1)\dfrac{u}{K}\right]+\sqrt{\left[\beta\mp(1-\beta^2)\dfrac{u}{K}\right]^2-1}\right\}\end{cases}$$

$$\int u\,du\cosh^{-1}\left(\beta\mp\frac{K}{u}\right)=\frac{u^2}{2}\cosh^{-1}\left(\beta\mp\frac{K}{u}\right)+\begin{cases}\dfrac{K^2}{2(1-\beta^2)^{3/2}}\left\{\beta\sin^{-1}\left[(1-\beta^2)\dfrac{u}{K}\pm\beta\right]\pm\sqrt{1-\left[(1-\beta^2)\dfrac{u}{K}\pm\beta\right]^2}\right\}\\[2ex]\dfrac{K^2}{2(\beta^2-1)^{3/2}}\left\{-\beta\cosh^{-1}\left[(\beta^2-1)\dfrac{u}{K}\mp\beta\right]\mp\sqrt{\left[(\beta^2-1)\dfrac{u}{K}\mp\beta\right]^2-1}\right\}\end{cases}$$

$$\int du\sqrt{u^2-(K\mp\beta u)^2}=\begin{cases}\dfrac{\pm K^2}{2(1-\beta^2)^{3/2}}\left\{\left[\beta\pm(1-\beta^2)\dfrac{u}{K}\right]\sqrt{\left[\beta\pm(1-\beta^2)\dfrac{u}{K}\right]^2-1}-\cosh^{-1}\left[\beta\pm(1-\beta^2)\dfrac{u}{K}\right]\right\}\\[2ex]\dfrac{\mp K^2}{2(\beta^2-1)^{3/2}}\left\{\left[\beta\mp(\beta^2-1)\dfrac{u}{K}\right]\sqrt{1-\left[(\beta^2-1)\dfrac{u}{K}\mp\beta\right]^2}+\sin^{-1}\left[\beta\mp(\beta^2-1)\dfrac{u}{K}\right]\right\}\end{cases}$$

$$\int du\sqrt{u^2-(\beta u\mp K)^2}=\begin{cases}\dfrac{K^2}{2(1-\beta^2)^{3/2}}\left\{\left[(1-\beta^2)\dfrac{u}{K}\pm\beta\right]\sqrt{\left[(1-\beta^2)\dfrac{u}{K}\pm\beta\right]^2-1}-\cosh^{-1}\left[(1-\beta^2)\dfrac{u}{K}\pm\beta\right]\right\}\\[2ex]\dfrac{K^2}{2(\beta^2-1)^{3/2}}\left\{\left[(\beta^2-1)\dfrac{u}{K}\mp\beta\right]\sqrt{1-\left[(\beta^2-1)\dfrac{u}{K}\mp\beta\right]^2}+\sin^{-1}\left[(\beta^2-1)\dfrac{u}{K}\mp\beta\right]\right\}\end{cases}$$

$$\int du\sqrt{(K\mp\beta u)^2-u^2}=\begin{cases}\dfrac{\pm K^2}{2(1-\beta^2)^{3/2}}\left\{\left[\beta\pm(1-\beta^2)\dfrac{u}{K}\right]\sqrt{1-\left[\beta\pm(1-\beta^2)\dfrac{u}{K}\right]^2}+\sin^{-1}\left[\beta\pm(1-\beta^2)\dfrac{u}{K}\right]\right\}\\[2ex]\dfrac{\mp K^2}{2(\beta^2-1)^{3/2}}\left\{\left[\beta\mp(\beta^2-1)\dfrac{u}{K}\right]\sqrt{\left[\beta\mp(\beta^2-1)\dfrac{u}{K}\right]^2-1}-\cosh^{-1}\left[\beta\mp(\beta^2-1)\dfrac{u}{K}\right]\right\}\end{cases}$$

$$\int du\sqrt{(\beta u\mp K)^2-u^2}=\begin{cases}\dfrac{K^2}{2(1-\beta^2)^{3/2}}\left\{\left[(1-\beta^2)\dfrac{u}{K}\pm\beta\right]\sqrt{1-\left[(1-\beta^2)\dfrac{u}{K}\pm\beta\right]^2}+\sin^{-1}\left[(1-\beta^2)\dfrac{u}{K}\pm\beta\right]\right\}\\[2ex]\dfrac{K^2}{2(\beta^2-1)^{3/2}}\left\{\left[(\beta^2-1)\dfrac{u}{K}\mp\beta\right]\sqrt{\left[(\beta^2-1)\dfrac{u}{K}\mp\beta\right]^2-1}-\cosh^{-1}\left[(\beta^2-1)\dfrac{u}{K}\mp\beta\right]\right\}\end{cases}$$

$$\int u\,du\left\{\left(\frac{K}{u}\mp\beta\right)\cosh^{-1}\left(\frac{K}{u}\mp\beta\right)-\sqrt{\left(\frac{K}{u}\mp\beta\right)^2-1}\right\}=\left(K\mp\frac{\beta u}{2}\right)u\cosh^{-1}\left(\frac{K}{u}\mp\beta\right)$$
$$+\begin{cases}\dfrac{\pm K^2}{2(1-\beta^2)^{1/2}}\sin^{-1}\left[\beta\pm(1-\beta^2)\dfrac{u}{K}\right]+\dfrac{-Ku}{2(1-\beta^2)^{1/2}}\sqrt{1-\left[\beta\pm(1-\beta^2)\dfrac{u}{K}\right]^2}\\[2ex]\dfrac{\mp K^2}{2(\beta^2-1)^{1/2}}\cosh^{-1}\left[\beta\mp(\beta^2-1)\dfrac{u}{K}\right]+\dfrac{-Ku}{2(\beta^2-1)^{1/2}}\sqrt{\left[\beta\mp(\beta^2-1)\dfrac{u}{K}\right]^2-1}\end{cases}$$

$$\int_0^\infty \frac{J_0(at)\,(1-\cos bt)}{t}\,dt = \begin{cases} \sin^{-1}\frac{b}{a} & (a>b) \\ \cosh^{-1}\frac{b}{a} & (b>a) \end{cases}$$

$$\int_0^\infty \frac{J_1(at)\sin bt}{t}\,dt = \begin{cases} \frac{b}{a} & (a>b) \\ \frac{b-\sqrt{b^2-a^2}}{a} & (b>a) \end{cases}$$

$$\int_0^\infty J_1(at)\,(1-\cos bt)\,\frac{dt}{t^2} = \begin{cases} \frac{a}{2} & (a>b) \\ \frac{a}{2}\cosh^{-1}\frac{b}{a} + \frac{b}{2a}\left(b-\sqrt{b^2-a^2}\right) & (b>a) \end{cases}$$

$$\int_0^\infty Y_0(at)\sin bt\,\frac{dt}{t} = \begin{cases} 0 & (a>b) \\ -\cosh^{-1}\frac{b}{a} & (b>a) \end{cases}$$

$$\int_0^\infty Y_0(at)\,(1-\cos bt)\,\frac{dt}{t} = \begin{cases} \frac{1}{\pi}\left(\sin^{-1}\frac{b}{a}\right)^2 & (a\geq b) \\ \frac{1}{\pi}\left[\frac{\pi^2}{4}-\left(\cosh^{-1}\frac{b}{a}\right)^2\right] & (b\geq a) \end{cases}$$

$$\int_0^\infty Y_1(at)\,(1-\cos bt)\,\frac{dt}{t} = \begin{cases} 0 & (a>b) \\ -\frac{\sqrt{b^2-a^2}}{a} & (b>a) \end{cases}$$

$$\int \frac{\sqrt{(t_1-\beta_1\eta)^2-(y-\eta)^2}}{(y-\eta)^2}\,d\eta = \int \frac{\sqrt{N}}{(y-\eta)^2}\,d\eta = \frac{\sqrt{N}}{y-\eta} + \beta_1 \cosh^{-1}\frac{t_1-\beta_1\eta}{y-\eta} + \begin{cases} \sqrt{\beta_1^2-1}\,\cosh^{-1}\frac{(\beta_1^2-1)\eta+y-\beta_1 t_1}{t_1-\beta_1 y} \\ \sqrt{1-\beta_1^2}\,\sin^{-1}\frac{(\beta_1^2-1)\eta+y-\beta_1 t_1}{t_1-\beta_1 y} \end{cases}^*$$

$$\int \frac{\sqrt{(t_1-\beta_1\eta)^2-(y+\eta)^2}}{(y+\eta)^2}\,d\eta = \int \frac{\sqrt{N'}}{(y+\eta)^2}\,d\eta = \frac{-\sqrt{N'}}{y+\eta} - \beta_1 \cosh^{-1}\frac{t_1-\beta_1\eta}{y+\eta} + \begin{cases} \sqrt{\beta_1^2-1}\,\cosh^{-1}\frac{(\beta_1^2-1)\eta-(y+\beta_1 t_1)}{t_1+\beta_1 y} \\ \sqrt{1-\beta_1^2}\,\sin^{-1}\frac{(\beta_1^2-1)\eta-(y+\beta_1 t_1)}{t_1+\beta_1 y} \end{cases}^*$$

*Use upper line if $\beta_1 > 1$, lower line if $\beta < 1$. Similar integrals for β_0 are obtained by substituting t_0 for t_1, β_0 for β_1.

Appendix C

Nomenclature

a	velocity of sound
a_o	half root chord
a_o'	$\frac{a_o}{m'}$
a_t	half tip chord
a_t'	$\frac{a_t}{m'}$
a_y	half chord at y, $a_o - \nu(y)$
a_y'	$\frac{a_y}{m'}$
AR	aspect ratio, $\frac{2b}{a_o + a_t}$
b	half span
b'	$\frac{b}{a_o'} = \frac{1+\sigma}{2\beta} AR \tan\gamma$
C	chord
C_D	wave drag coefficient
C_{D_o}	2-dimensional wave drag coefficient, $\frac{4\alpha_o^2}{m'}$
C_L	lift coefficient
C_M	moment coefficient
C_p	pressure coefficient
C_{p_o}	2-dimensional pressure coefficient or assigned pressure coefficient
D	wave drag
$F(\lambda,\eta)$	distribution function of the harmonic source (complex). See Eq. (2.5)
$f(\lambda,\eta)$	$-\frac{1}{4} F(\lambda,\eta)$

$G(\lambda,\eta)$	doublet distribution function (complex) See Eq. (2.7)
$g(\lambda,\eta)$	$\frac{i\lambda G(\lambda,\eta)}{\beta m'}$
$H_0^{(1)}$	Hankel function of the first kind of zero order
$H_0^{(2)}$	Hankel function of the second kind of zero order
$H_1^{(1)}$	Hankel function of the first kind of first order
$H_1^{(2)}$	Hankel function of the second kind of first order
$\overline{H_1^{(2)}}$	$J_1(\ )+iY_1(\ )$ = conjugate of $H_1^{(2)}(\ )$
J_0	Bessel function of zero order
J_1	Bessel function of first order
M	Mach number
m'	$\sqrt{M^2-1}$
p	pressure
p_o	free stream static pressure
r	$\sqrt{(y-\eta)^2+z^2}$
t	$\frac{x}{m'}$, longitudinal coordinate in transformed plane (equivalent to time in supersonic case).
t_o	$t+a_o'$
t_1	$t-a_o'$
U	free stream velocity
u	velocity component in x (or t) direction
v	velocity component in y direction
w	velocity component in z direction
x	longitudinal axis

y	spanwise axis
y'	$\frac{y}{a_o'}$
Y_o	Bessel function of the second kind of zero order
Y_1	Bessel function of the second kind of first order
z	vertical axis
α	angle of attack
α_+	angle of attack of upper surface of airfoil
α_-	angle of attack of lower surface of airfoil
α_o	slope of upper surface on symmetrical airfoil
α_1	angle of attack of cambered wing
β	$\frac{\tan\delta}{m'} = \tan\gamma'$
β_o	$\beta + \nu'$
β_1	$\beta - \nu'$
γ	angle between mid-chord line and y-axis (x, y plane)
γ'	angle between mid-chord line and y-axis (t, y plane)
γ_o	leading edge sweep-back angle (x, y plane)
γ_1	trailing edge sweep-back angle (x, y plane)
η	source location along y-axi
μ	$\frac{b}{a_o}$
ν	$\frac{a_o - a_t}{b}$
ν'	$\frac{\nu}{m'} = \frac{1-\sigma}{b'}$

ξ	source location along x-axis (t-axis)
ρ_o	free stream density
σ	a_t/a_o , taper ratio
τ	$\frac{\xi}{m'}$
ϕ	velocity potential
ω	$\mu \tan\gamma$
ω_o	$\mu \tan\gamma_o$
ω_1	$\mu \tan\gamma_1$

LIST OF FIGURES

Fig. 9 The downwash distribution on and behind the swept-back wing at the nose (swept-back angle = 30° and the chord is unity) with assigned constant pressure coefficient C_{p_o} on the wing.

Fig. 10 The downwash distribution in the plane of the Delta wing at different locations along the span with assigned constant pressure coefficient C_{p_o} on the wing.

Fig. 11 The downwash distribution in the plane of a tapered swept-back wing with supersonic trailing edge and assigned constant pressure coefficient C_{p_o} on the wing.

Fig. 12 The same as Fig. 11 except showing downwash far downstream.

Fig. 1

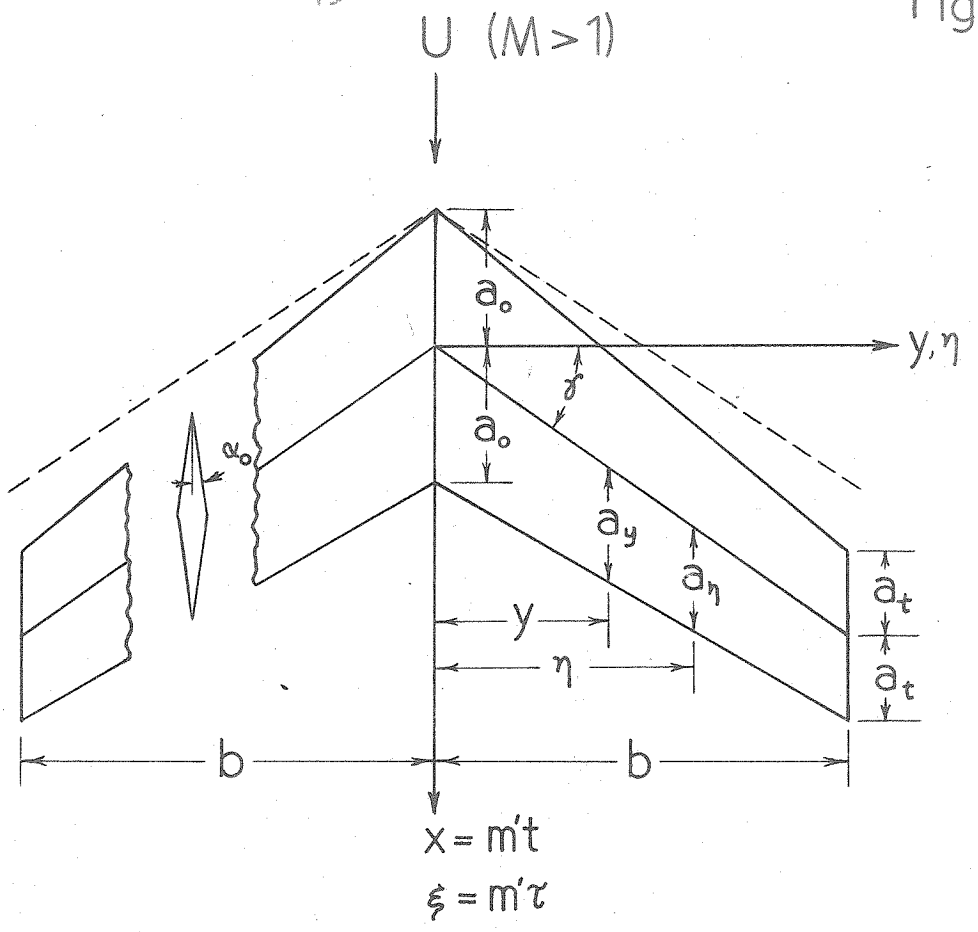

(a) Swept-back wing in physical plane (x,y)

a_o = half root chord	$a_o' = \frac{a_o}{m'}$ $\quad a_t' = \frac{a_t}{m'}$
a_t = half tip chord	$b' = \frac{b}{a_o'} = \frac{1+\sigma}{2\beta} \cdot AR\tan\gamma$
b = half span	$\beta = \frac{\tan\gamma}{m'}$
$\tan\gamma$	$\nu' = \frac{\nu}{m'} = \frac{1-\sigma}{b'} = \frac{2\beta}{AR\tan\gamma}\ \frac{1-\sigma}{1+\sigma}$
$\nu = \frac{a_o - a_t}{b}$	
$a_y = a_o - \nu y$	$a' = a_y/m'$
$\sigma = a_t/a_o$ = taper ratio	$\sigma = 1 - \nu' b'$
$AR = \frac{2b}{a_o + a_t}$ = aspect ratio	$AR = \frac{2b'}{m'(1+\sigma)}$
$m' = \sqrt{M^2-1}$	$\beta_1 = \beta - \nu'$
α_o = surface slope	$\beta_o = \beta + \nu'$

(b) Parameter relations between physical plane (x,y)

and transformed plane (t,y)

Fig. 1

(c) Swept-back wing in transformed plane (t,y)

(Note: Mach line at 45°)

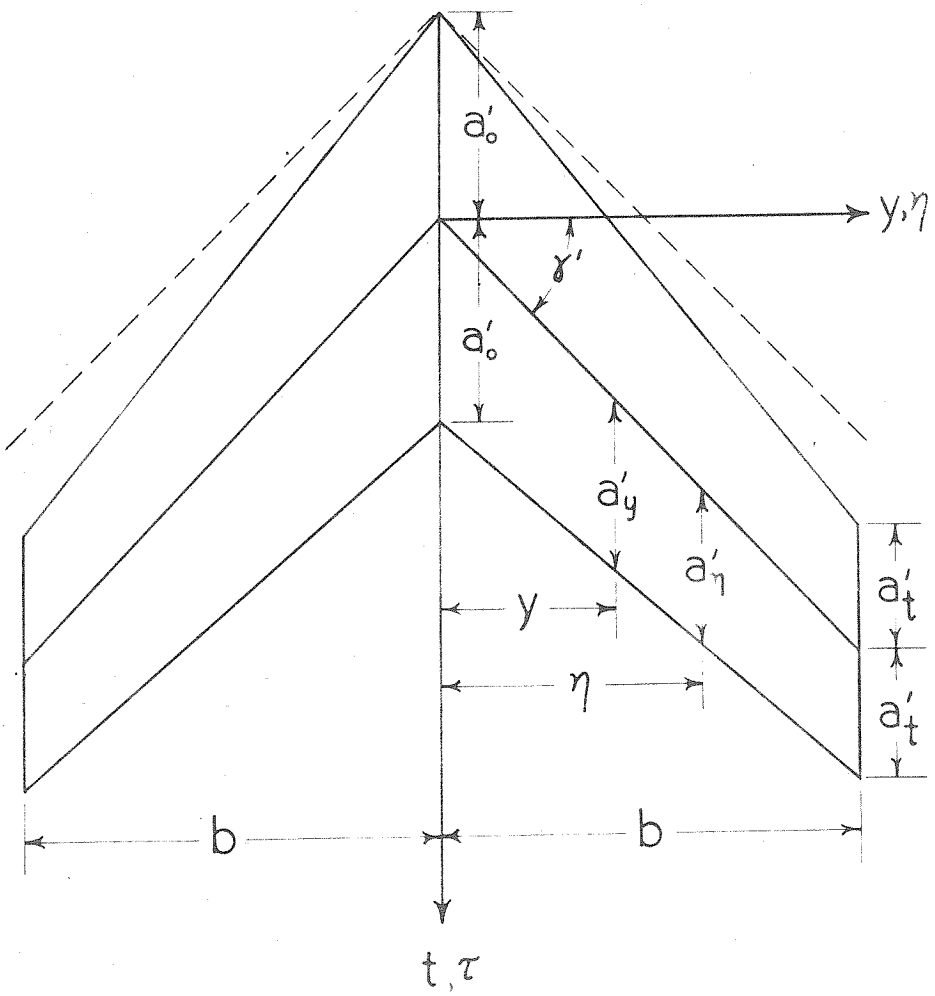

Fig. 2

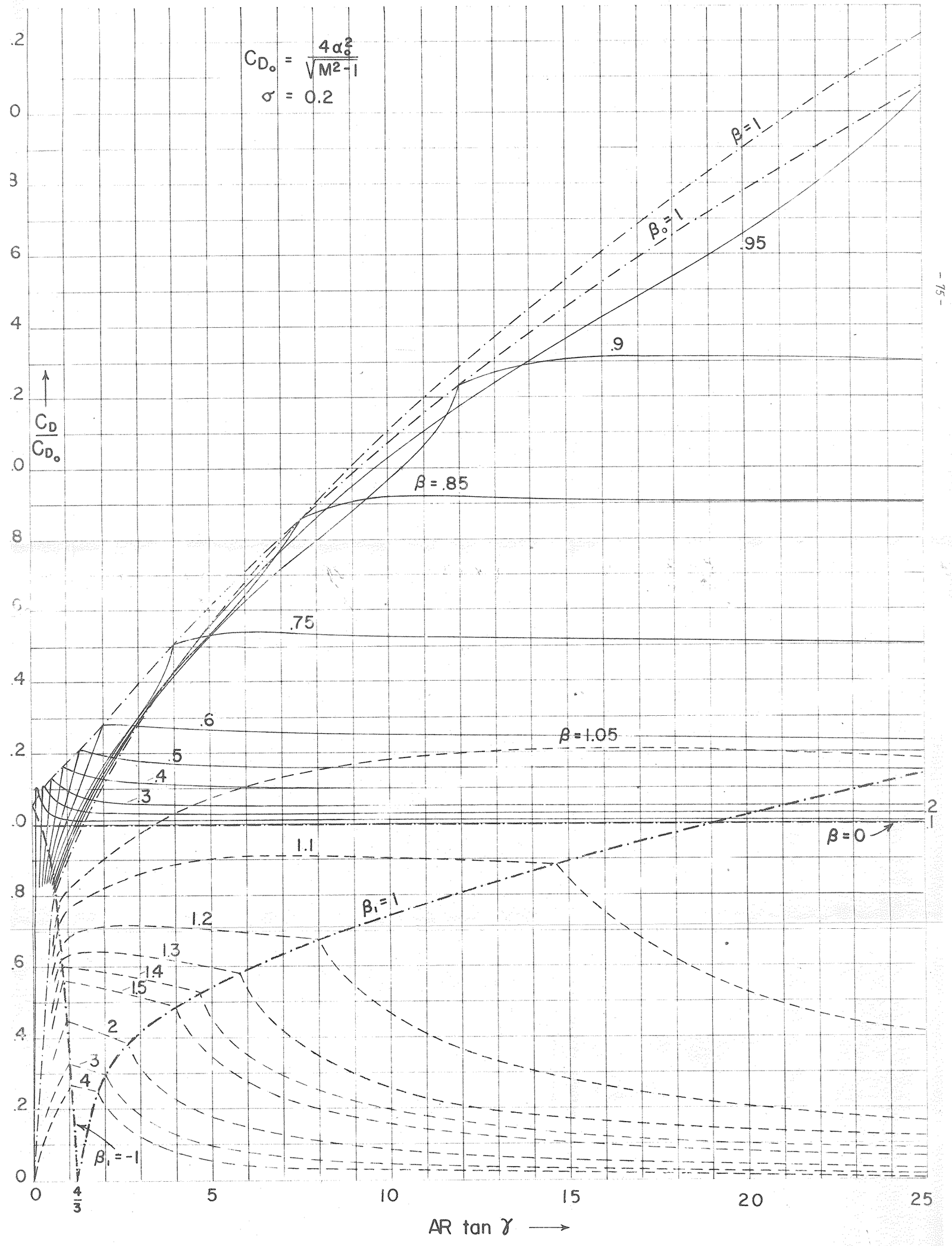
$C_{D_o} = \frac{4\alpha_o^2}{\sqrt{M^2-1}}$
$\sigma = 0.2$
$\frac{C_D}{C_{D_o}}$
$\beta = 1$
$\beta_o = 1$
.95
.9
$\beta = .85$
.75
.6
.5
.4
.3
$\beta = 1.05$
2
1
$\beta = 0$
1.1
$\beta_1 = 1$
1.2
1.3
1.4
1.5
2
3
4
$\beta_1 = -1$
0
$\frac{4}{3}$
5
10
15
20
25
AR tan γ ⟶

Fig. 3

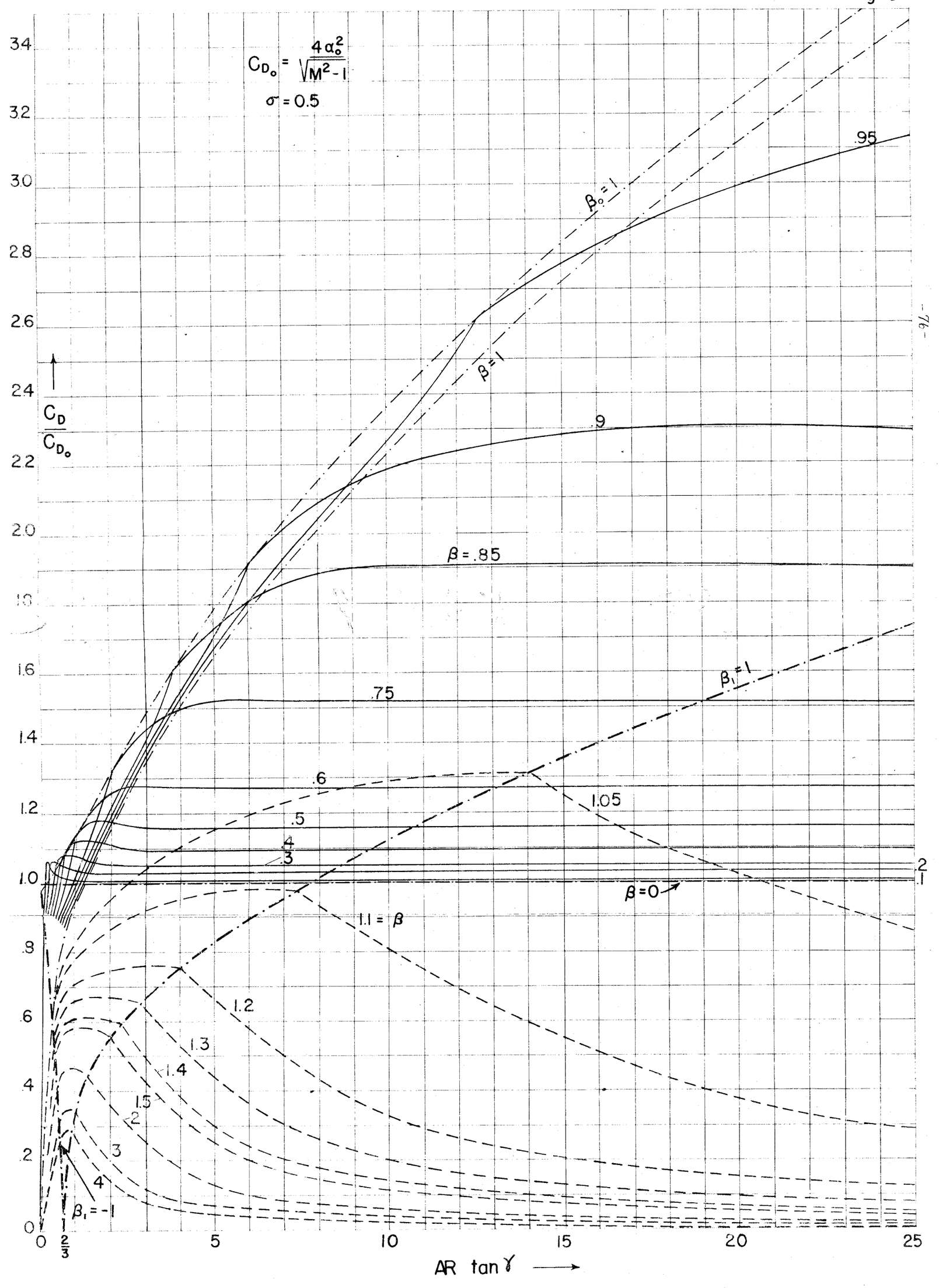
$C_{D_o} = \frac{4\alpha_o^2}{\sqrt{M^2-1}}$
$\sigma = 0.5$
$\frac{C_D}{C_{D_o}}$
$\beta_o = 1$
$\beta = 1$
.95
.9
$\beta = .85$
$\beta_1 = 1$
.75
.6
1.05
.5
4/3
2
1
$\beta = 0$
1.1 = β
1.2
1.3
1.4
1.5
2
3
4
$\beta_1 = -1$
0
2/3
5
10
15
20
25
AR tan γ ⟶

Fig. 4

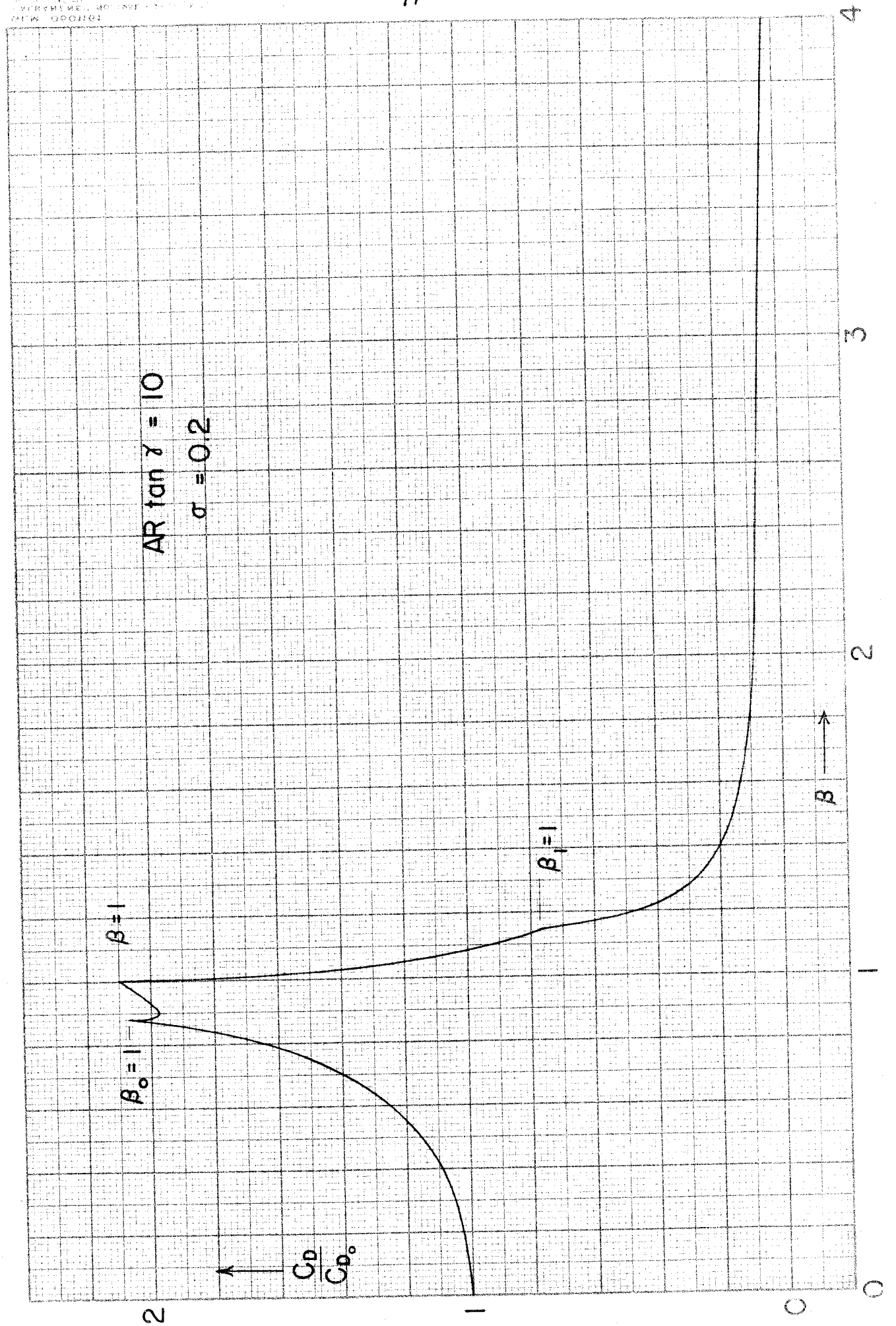

Fig. 5

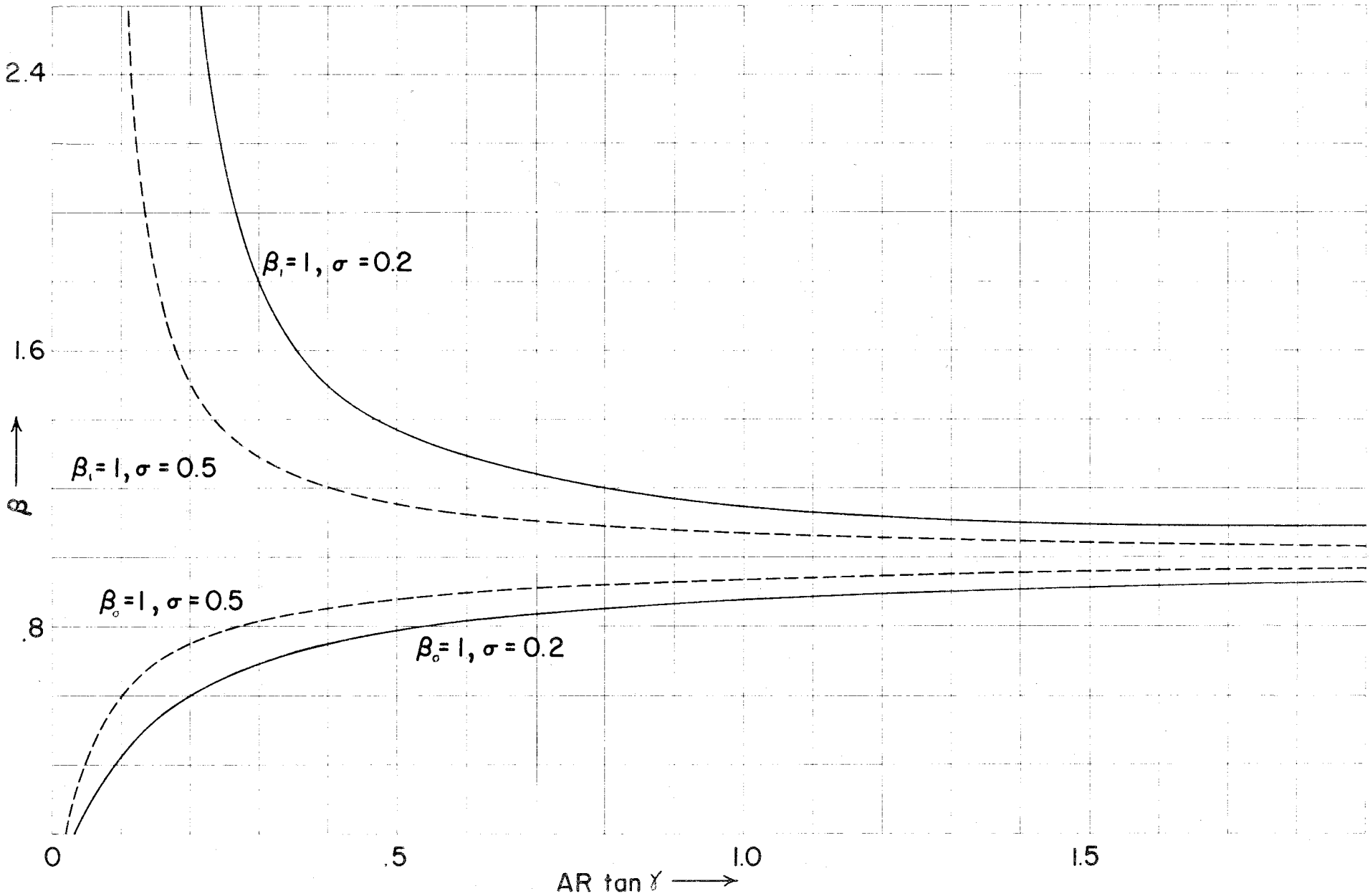
2.4
1.6
.8
$\beta_i = 1, \sigma = 0.2$
$\beta_i = 1, \sigma = 0.5$
$\beta_o = 1, \sigma = 0.5$
$\beta_o = 1, \sigma = 0.2$
β
0
.5
1.0
1.5
AR tan γ ⟶

A-9

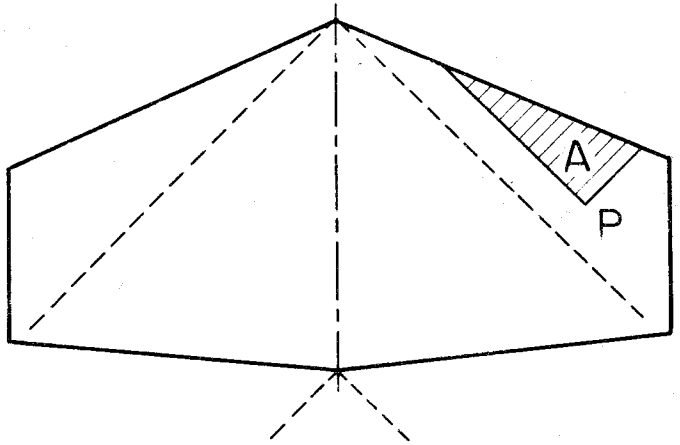

(a)

A-1, C-1

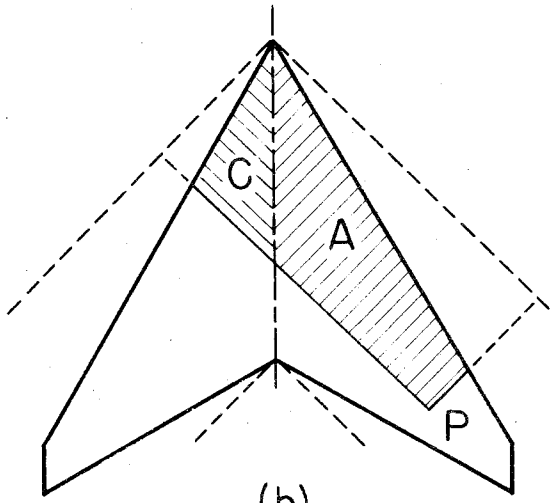

(b)

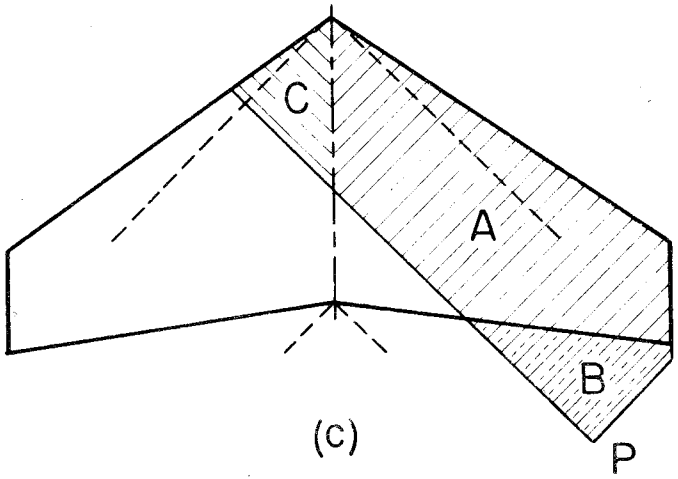

(c)

A-8, B-10, C-3

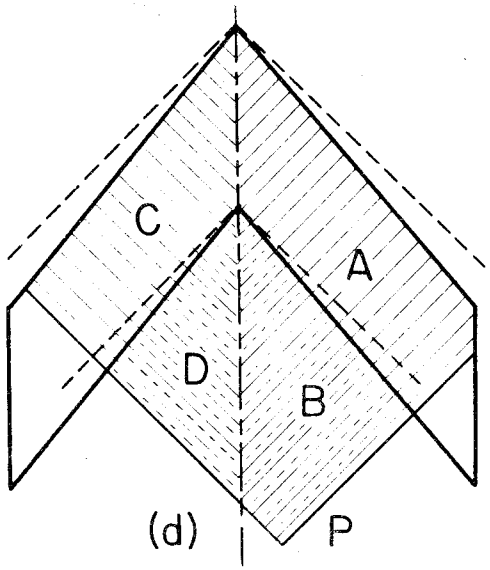

(d)

A-2, B-1, C-1, D-1

Fig. 7a

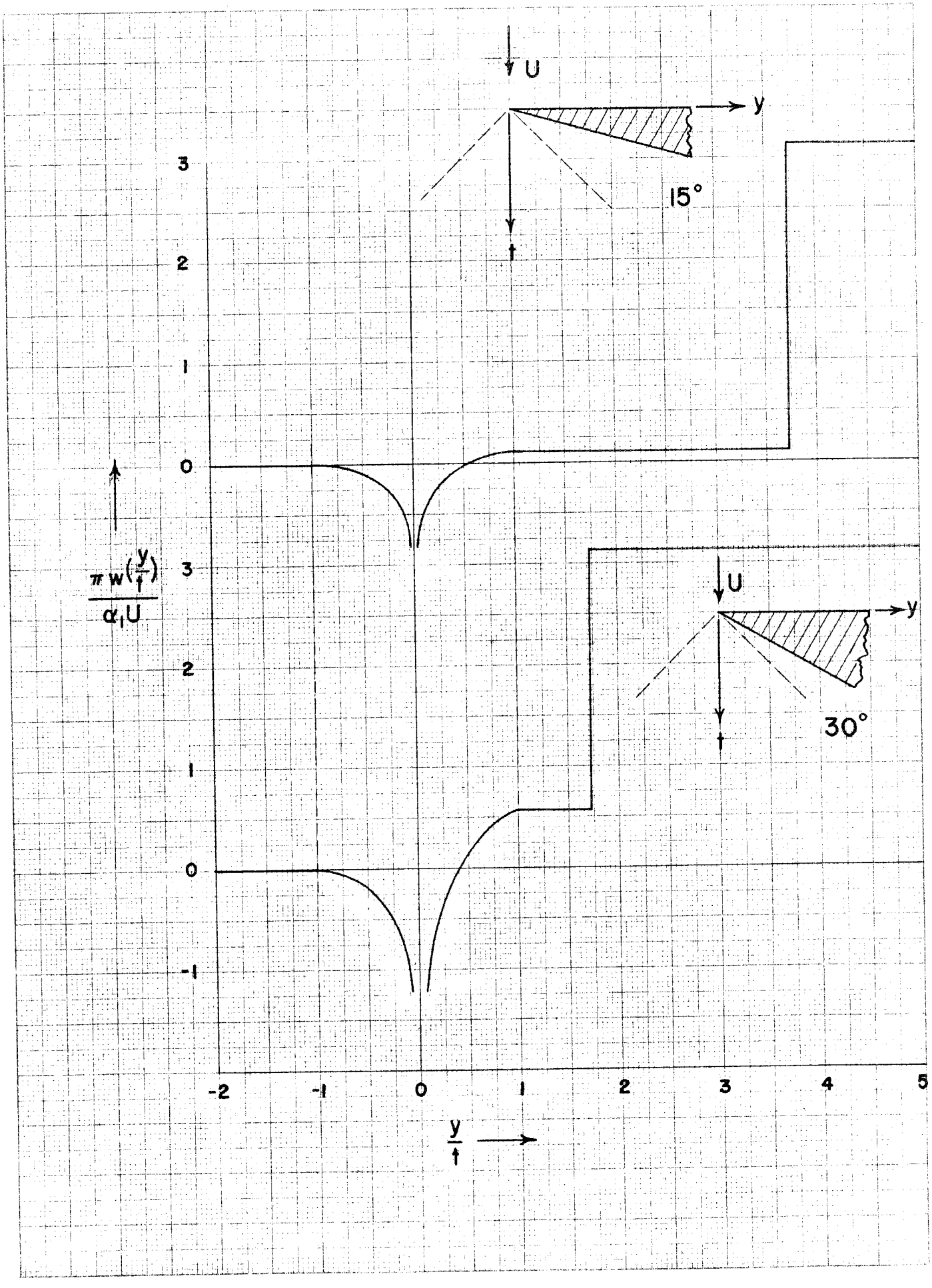
U
y
15°
t
3
2
1
0
$\frac{\pi w(\frac{y}{t})}{\alpha_1 U}$
U
y
30°
t
3
2
1
0
-1
-2
-1
0
1
2
3
4
5
$\frac{y}{t}$

Fig. 7b

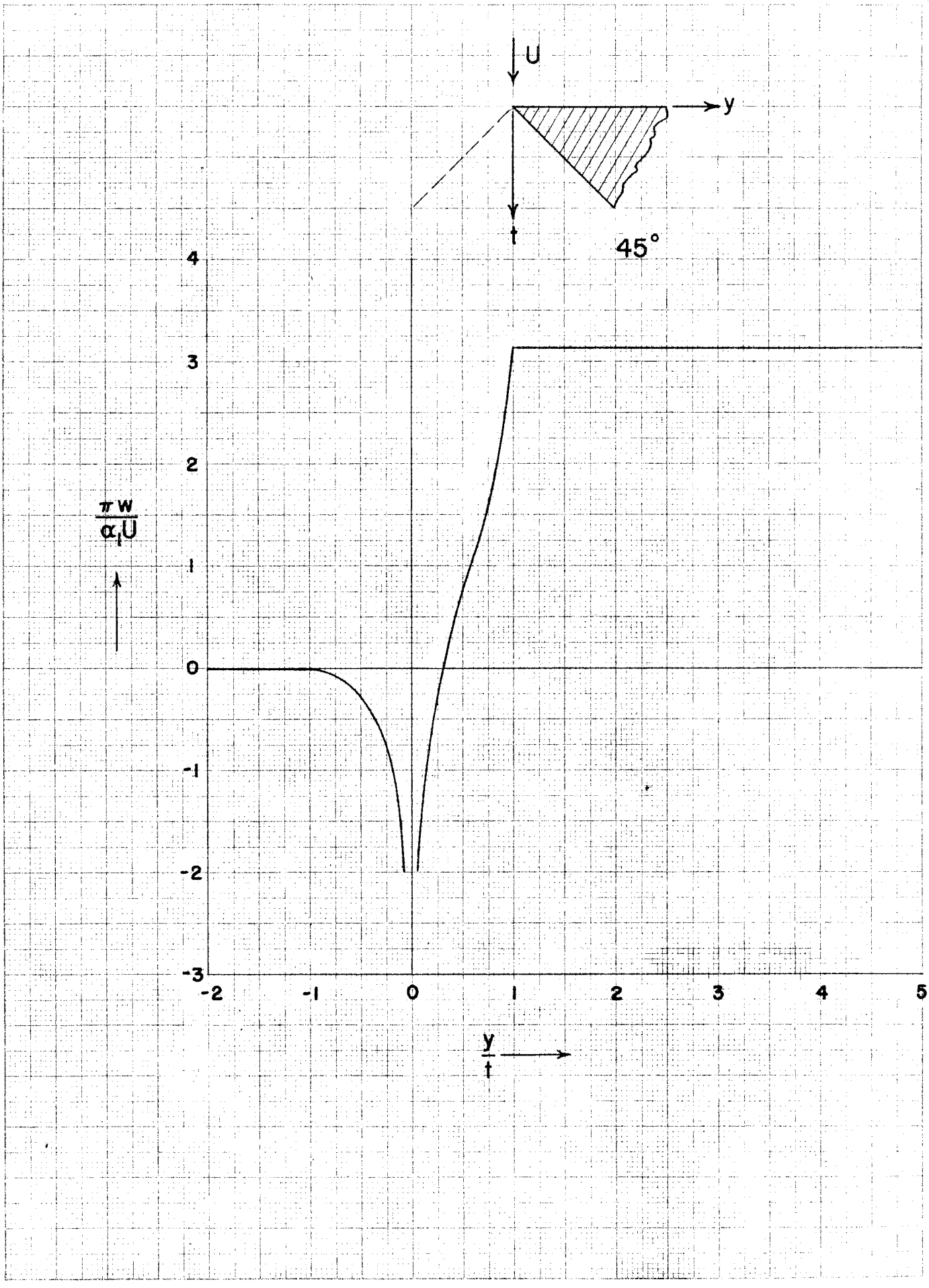

Fig. 8

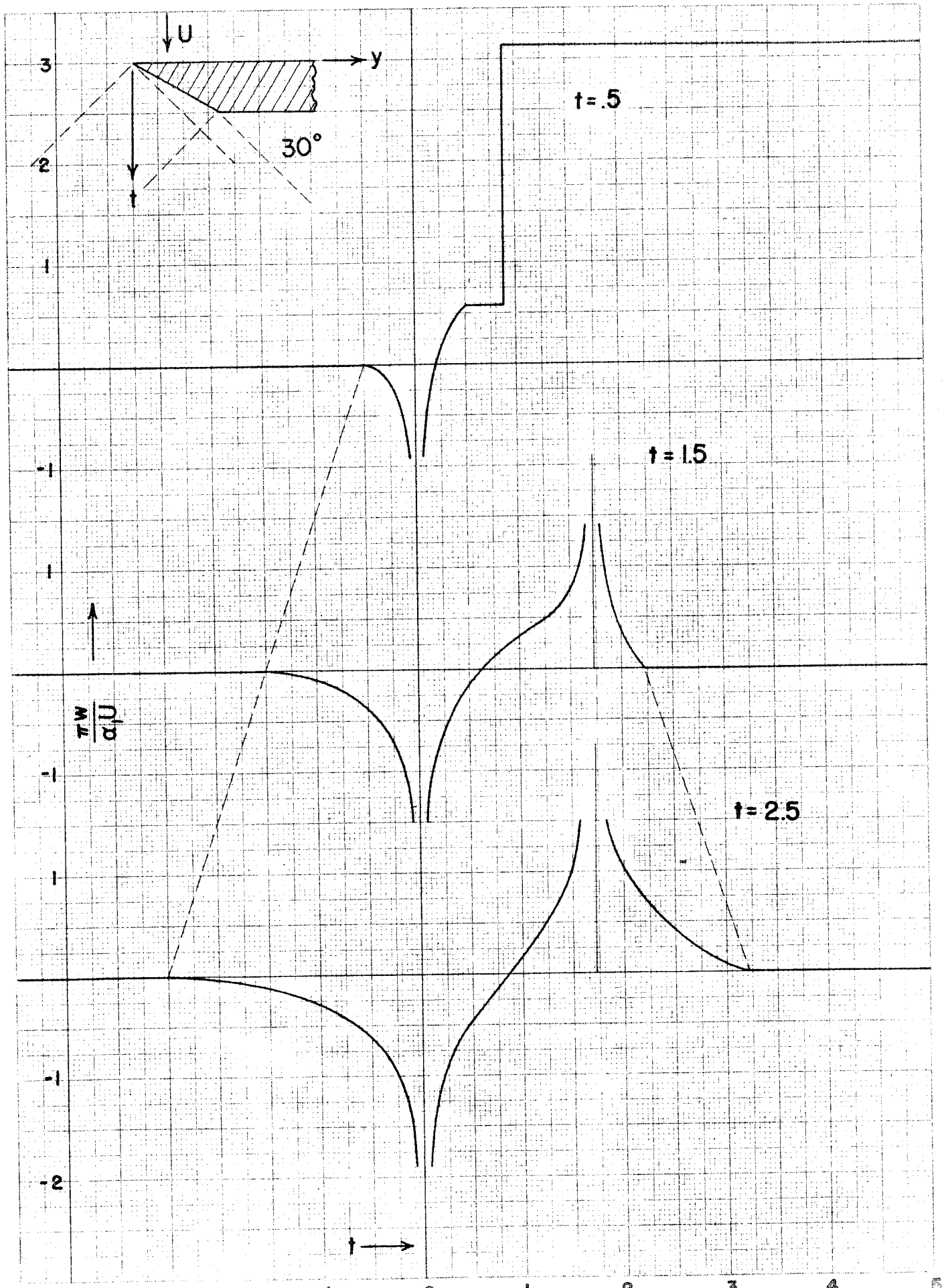

Fig. 9

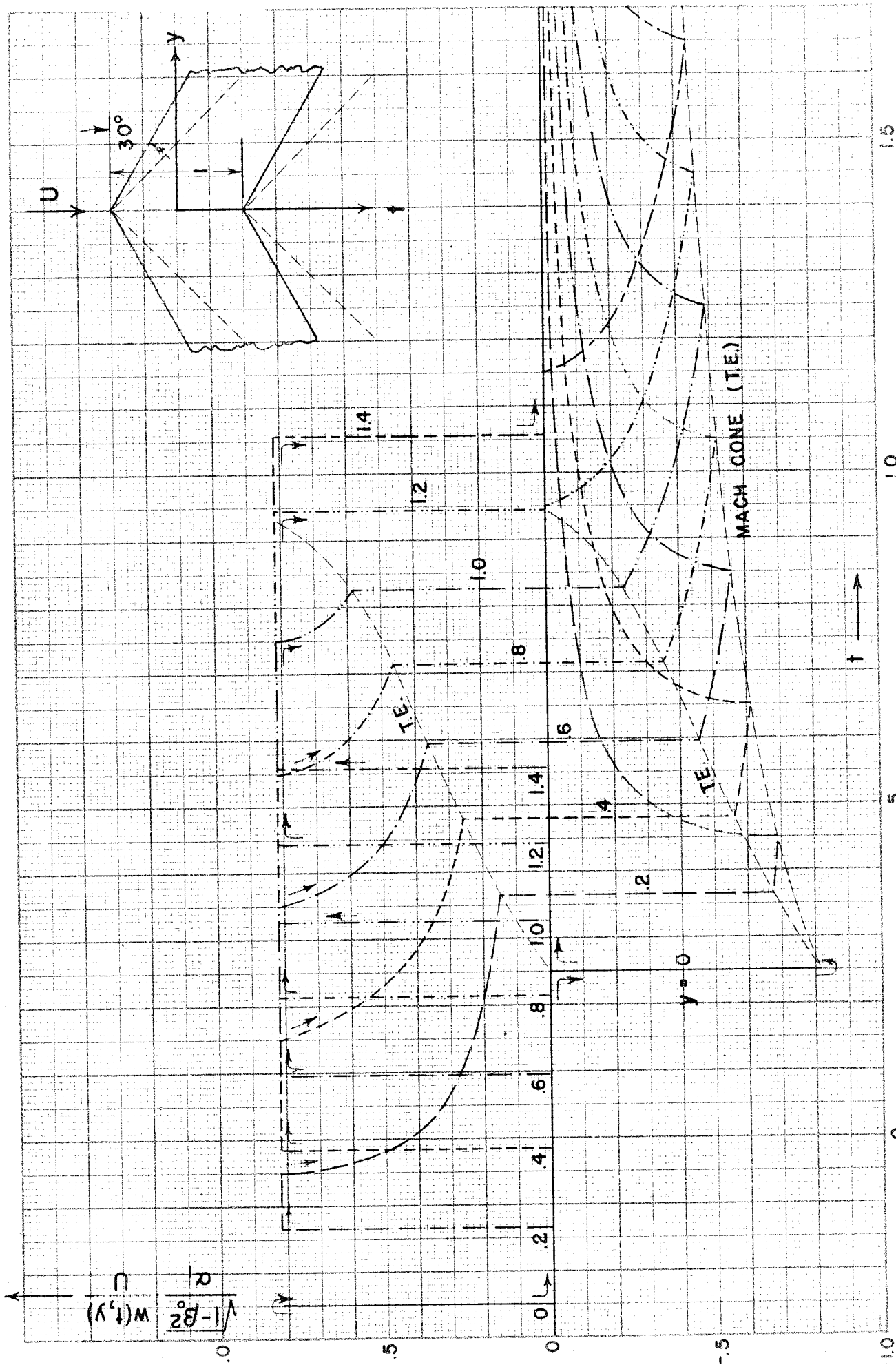
$C_{P_o} = \frac{2\alpha_1}{m'\sqrt{1-\beta_o^2}}$
$\beta_o = \tan 30°$
$\frac{\sqrt{1-\beta_o^2}}{\alpha_1} \frac{w(1,y)}{U}$
U
30°
y
t
T.E.
T.E.
MACH CONE (T.E.)
y = 0
t
1.5
1.0
.5
0
-.5
-1.0
0
.2
.4
.6
.8
1.0
1.2
1.4
.2
.4
.6
.8
1.0
1.2
1.4

Fig. 1C

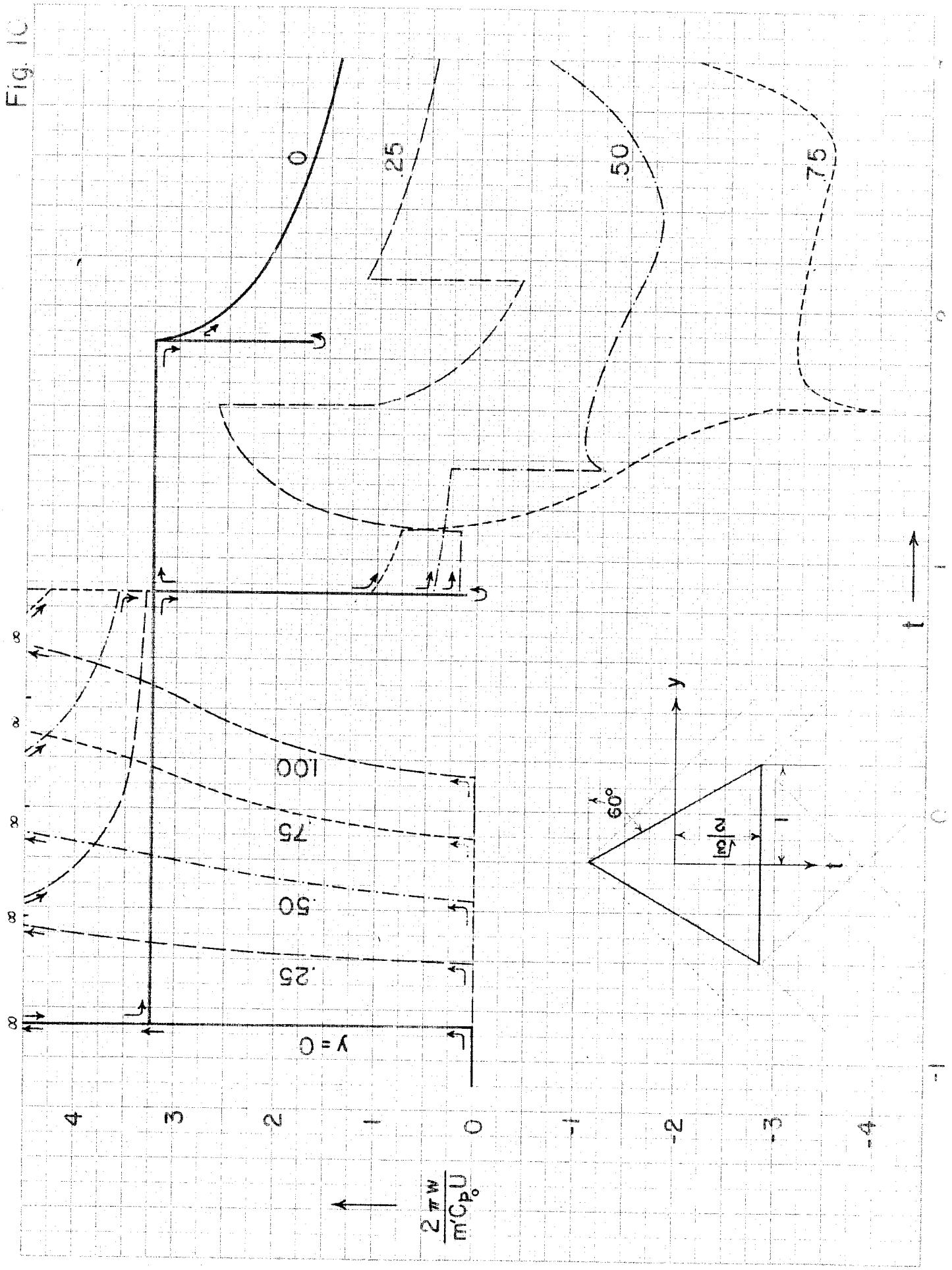
0
25
50
75
100
75
50
25
y = 0
60°
y
t
$\frac{\sqrt{3}}{2}$
1
$\frac{2\pi w}{m'C_{p_0}U}$
4
3
2
1
0
-1
-2
-3
-4

Fig. 11

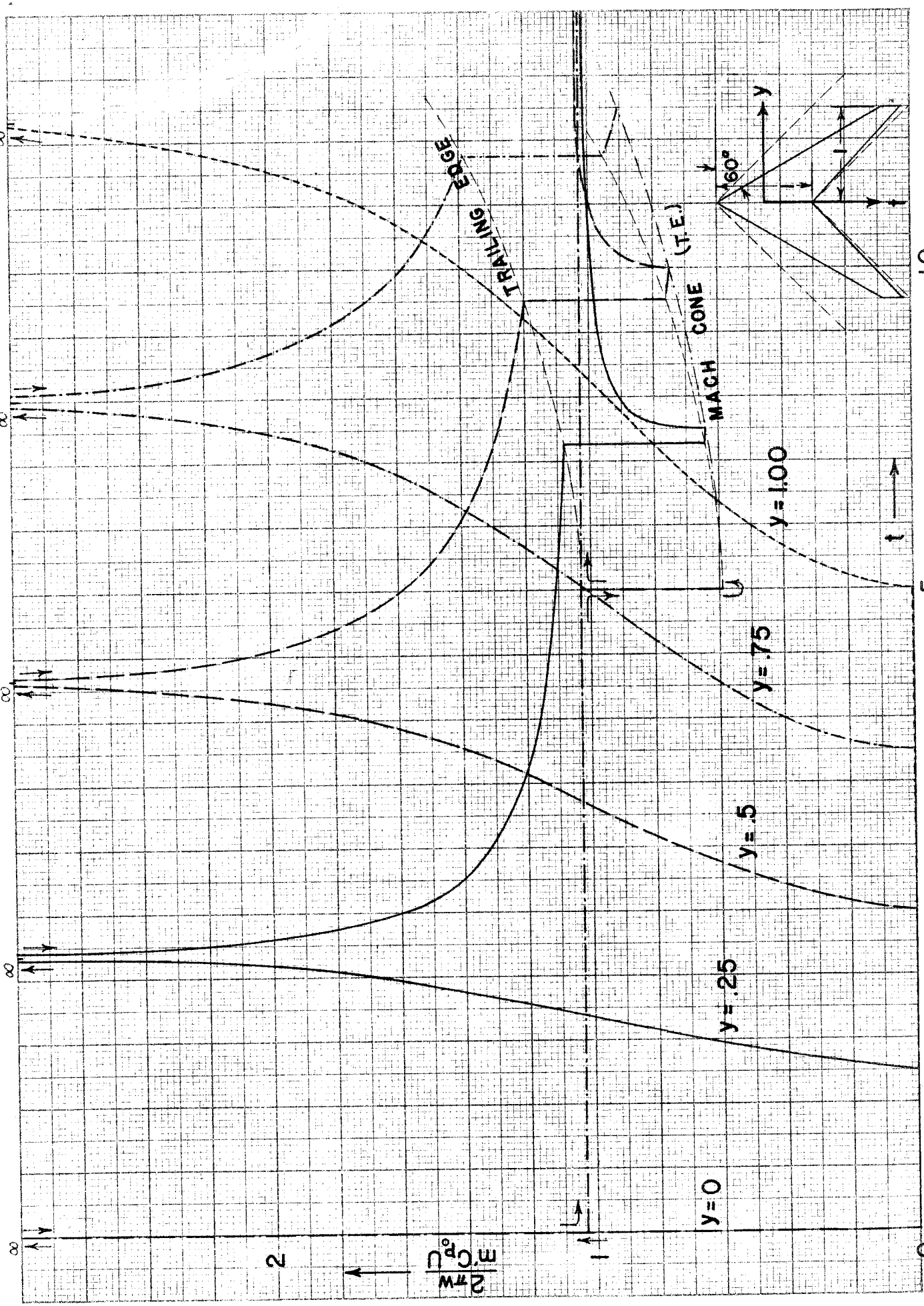
$\frac{2\pi w}{\pi C_{p_0} U}$
2
1
0
-.5
.5
1.0
t
y=0
y=.25
y=.5
y=.75
y=1.00
MACH CONE
(T.E.)
TRAILING EDGE
60°
y
t
1
∞

Fig. 12